



Originally published as:

Nowaczyk, N., Frederichs, T. W., Eisenhauer, A., Gard, G. (1994): Magnetostratigraphic data from late Quaternary sediments from the Yermak Plateau, Arctic Ocean: Evidence for four geomagnetic polarity events within the last 170 Ka of the Brunhes Chron. - *Geophysical Journal International*, 117, 2, pp. 453—471.

DOI: <https://doi.org/10.1111/j.1365-246X.1994.tb03944.x>

Magnetostratigraphic data from late Quaternary sediments from the Yermak Plateau, Arctic Ocean: evidence for four geomagnetic polarity events within the last 170 Ka of the Brunhes Chron

Norbert R. Nowaczyk,^{1,*} Thomas W. Frederichs,¹ Anton Eisenhauer² and Gunilla Gard³

¹Fachbereich Geowissenschaften, Universität Bremen, D-28344 Bremen, Germany

²Heidelberger Akademie der Wissenschaften, Institut für Umweltpophysik
D-69120 Heidelberg, Germany

³Department of Geology and Geochemistry, University of Stockholm, S-10691 Stockholm, Sweden

Accepted 1993 October 6. Received 1993 October 4; in original form 1993 June 2

SUMMARY

Palaeomagnetic investigations of two sediment cores recovered from RV *Polarstern* near the eastern slope of the Yermak Plateau (sites PS 1533 and PS 2212) reveal convincing evidence for four polarity events of the Earth's magnetic field during the last 170 Ka. A comprehensive rock magnetic study of the sediments proved that fine-grained magnetite is the principal carrier of the remanent magnetization. No changes in magneto-mineralogy across the polarity transitions in the sediments investigated were found. Calcareous nannofossil biostratigraphy, AMS-¹⁴C (accelerated mass spectrometry) and oxygen isotope data, and ¹⁰Be and ²³⁰Th stratigraphies yielded age ranges of 24–29 Ka for the Mono Lake event, 34–43 Ka for the Laschamp event, 72–86 Ka for the Norwegian–Greenland Sea event and 118–128 Ka for the Blake event. Two reverse polarity samples at the base of core PS 2212-3 KAL are interpreted as the termination of the Biwa I event (171–181 Ka). The events exhibit full inversion of inclination in both cores. The data suggest that the transition process of the Earth's magnetic field during such polarity events requires some 1 Ka.

Key words: alternating field demagnetization, Brunhes Chron, magnetostratigraphy, polarity events reversal process, Yermak Plateau.

INTRODUCTION

During the last 25 years a rising number of papers have reported short-term geomagnetic excursions and polarity events within the Brunhes Chron of normal polarity. Although contradictory results on sediments and volcanic rocks of the same age led to doubts about the reliability of postulated events (e.g. Verosub & Banerjee 1977; Hanna & Verosub 1989; Thouveny, Creer & Blunk 1990), recent reviews of formerly reported geomagnetic events and additional data have yielded an improved knowledge about these features of the geomagnetic field (Jacobs 1984; Champion, Lanphere & Kuntz 1988; Bleil & Gard 1989; Løvlie 1989; Nowaczyk & Baumann 1992).

Investigations of short geomagnetic events recorded in sediments at high latitudes can provide important

information about the stability and geometry of the geomagnetic field throughout the geologic past. The high intensity of the natural remanent magnetization allows a progressive demagnetization. Bioturbation affecting the sediments is very low or absent, which may preserve even thin layers of reversed magnetization directions. A detailed knowledge of the palaeomagnetic signature of geomagnetic events and the duration of the reversal process may lead to a better description and understanding of the processes generating the Earth's magnetic field (Bogue & Merrill 1992).

In this paper we present high-resolution magnetostratigraphies of late Quaternary deep-sea sediments recovered at the eastern slope of the Yermak Plateau from RV *Polarstern* during Arctic expeditions ARK IV/3 (Thiede *et al.* 1988; Krause, Meincke & Thiede 1989) and ARK VIII/3 'Arctic '91' (Fütterer *et al.* 1992). Two cores, PS 1533-3 SL and PS 2212-3 KAL (Fig. 1, Table 1), were studied for records of short-term polarity events within the

* Now at: GeoForschungsZentrum Potsdam, D-14473 Potsdam, Germany.

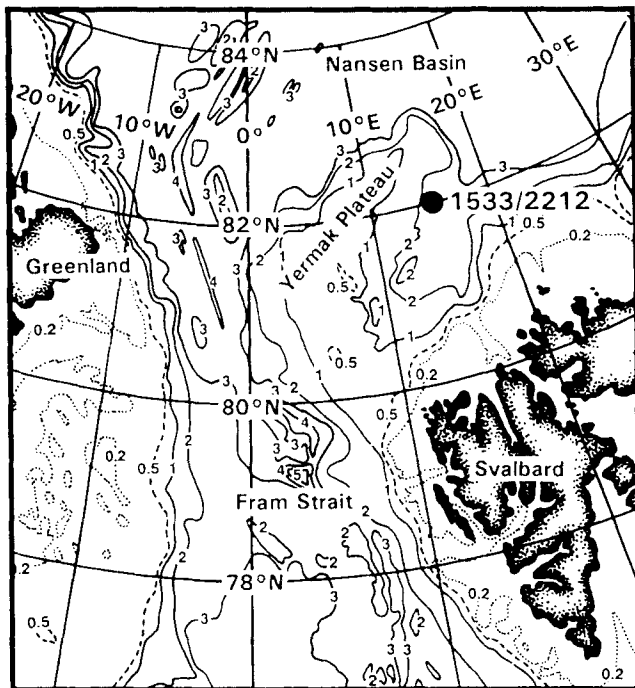


Figure 1. Location map of Polarstern sites PS 1533 (ARK IV/3) and PS 2212 (ARK VIII/3, Arctic'91). Depth intervals are in thousand metres. Bathymetric data after Perry *et al.* (1986).

Table 1. Location, water depth and length of the cores presented in this study.

Core-number	Type	Latitude	Longitude	Water Depth	Length
PS 1533-3	SL	82° 1.9' N	15° 10.7' E	2030 m	485 cm
PS 2212-3	KAL	82° 4.2' N	15° 51.2' E	2550 m	770 cm
SL	- 'Schwerelot'	: gravity corer		(ø = 12 cm)	
KAL	- 'Kastenlot'	: square barrel Kastenlot corer		(30 × 30 cm)	

Brunhes normal polarity Chron. Calcareous nannofossil (coccolith) biostratigraphies are available for core PS 1533-3 SL (Nowaczyk & Baumann 1992) and core PS 2212-3 KAL (this study). Further age control for core PS 1533-3 SL (Table 2) is provided by a ^{10}Be and ^{230}Th stratigraphy (this study; see also Hentschel 1992), a $\delta^{18}\text{O}$ stratigraphy and AMS- ^{14}C data by Köhler (1991). A detailed stratigraphic

Table 2. AMS- ^{14}C and $\delta^{18}\text{O}$ ages for core PS 1533-3 SL (Köhler 1991), and ages from $^{230}\text{Th}/^{10}\text{Be}$ stratigraphy (Hentschel 1992; this study).

Depth(interval) cm	Age ka	Dating Methods		
15-16	6.165 ± 0.08	AMS- ^{14}C		
32	12		$\delta^{18}\text{O}$	$^{230}\text{Th}/^{10}\text{Be}$
50	12			
84-85	17.87 ± 0.18	AMS- ^{14}C		
92-93	18.16 ± 0.13	AMS- ^{14}C		
110-111	22.79 ± 0.20	AMS- ^{14}C		
113	24		$\delta^{18}\text{O}$	
120	24			$^{230}\text{Th}/^{10}\text{Be}$
220	59			$^{230}\text{Th}/^{10}\text{Be}$
230	59		$\delta^{18}\text{O}$	
271	71		$\delta^{18}\text{O}$	
275	71			$^{230}\text{Th}/^{10}\text{Be}$
400	128			$^{230}\text{Th}/^{10}\text{Be}$
420	128		$\delta^{18}\text{O}$	

correlation of the cores is provided by high-resolution magnetic susceptibility measurements.

SAMPLING

During the Arctic expeditions ARK IV/3 and ARK VIII/3, two different large-diameter coring tools for the recovery of long sediment sections were used: a gravity corer (Schwerelot-SL) with an internal diameter of 12 cm, and a square-barrel Kastenlot corer (KAL) with an opening of 30 × 30 cm (Table 1). The recovered sediments are composed of brownish, greenish and greyish hemipelagic muds of terrigenous origin (sandy silt to silty clay) with only few biogenic relicts. A detailed sedimentological description of core PS 1533-3 SL is provided by Spielhagen, Pfirman & Thiede (1988) and of core PS 2212-3 KAL in Fütterer *et al.* (1992).

The palaeomagnetic sampling was carried out using cubic plastic boxes with a volume of 6.2 cm³. In general, the sampling interval was 5 cm for PS 1533-3 SL and 4 cm or less for PS 2212-3 KAL. A detailed description of the sampling technique is given by Nowaczyk & Baumann (1992).

PALAEOMAGNETISM

Measurements of the natural remanent magnetization (NRM) were carried out at the Fachbereich Geowissenschaften, Universität Bremen in Germany, using a three-axis cryogenic magnetometer (Cryogenics Consultants, Model GM 400) with a noise level of approximately 10^{-5} Am^{-1} . For intensities below 10^{-4} Am^{-1} , the remanence is determined by a special procedure which stacks measurements taken along four different orientations relative to the magnetometer's coordinate system. Samples with intensities down to $3 \times 10^{-5} \text{ Am}^{-1}$ can be used for palaeomagnetic interpretation.

Demagnetization was performed with single-axis alternating field (AF) demagnetizers, Schoenstedt GSD-1 (core PS 1533-3 SL) and 2G Enterprises (core PS 2212-3 KAL). In general, steps of 10, 20, 35, 50 and 65 mT were applied. If the maximum peak amplitude of 65 mT was not sufficient to isolate a single-component stable direction, additional steps of 80 and 100 mT or similar schemes (PS 2212-3 KAL up to 200 mT) were applied. For determining the direction of the characteristic remanent magnetization (ChRM), the quality criteria and methods described by Nowaczyk & Baumann (1992) were used.

The NRM intensities ranged between 1×10^{-3} and $3 \times 10^{-2} \text{ Am}^{-1}$, indicating a relatively strong magnetization with median destructive fields (MDF) of 10–30 mT. The magnetostratigraphic results of core PS 1533-3 SL have already been presented by Nowaczyk & Baumann (1992). Because of the high northern latitudes of the coring sites (82°N), the vertical component of the geomagnetic field dominates and the demagnetization results of core PS 2212-3 KAL are consequently discussed by the high-resolution downcore variations of the inclination only (Fig. 2a). In Fig. 2(a) the left column gives the NRM inclination, followed by the inclinations after the first four demagnetization steps in the middle and the ChRM inclinations in the right column. Fig. 2(b) gives the corresponding inclination logs of the difference vectors of the first four demagnetization steps.

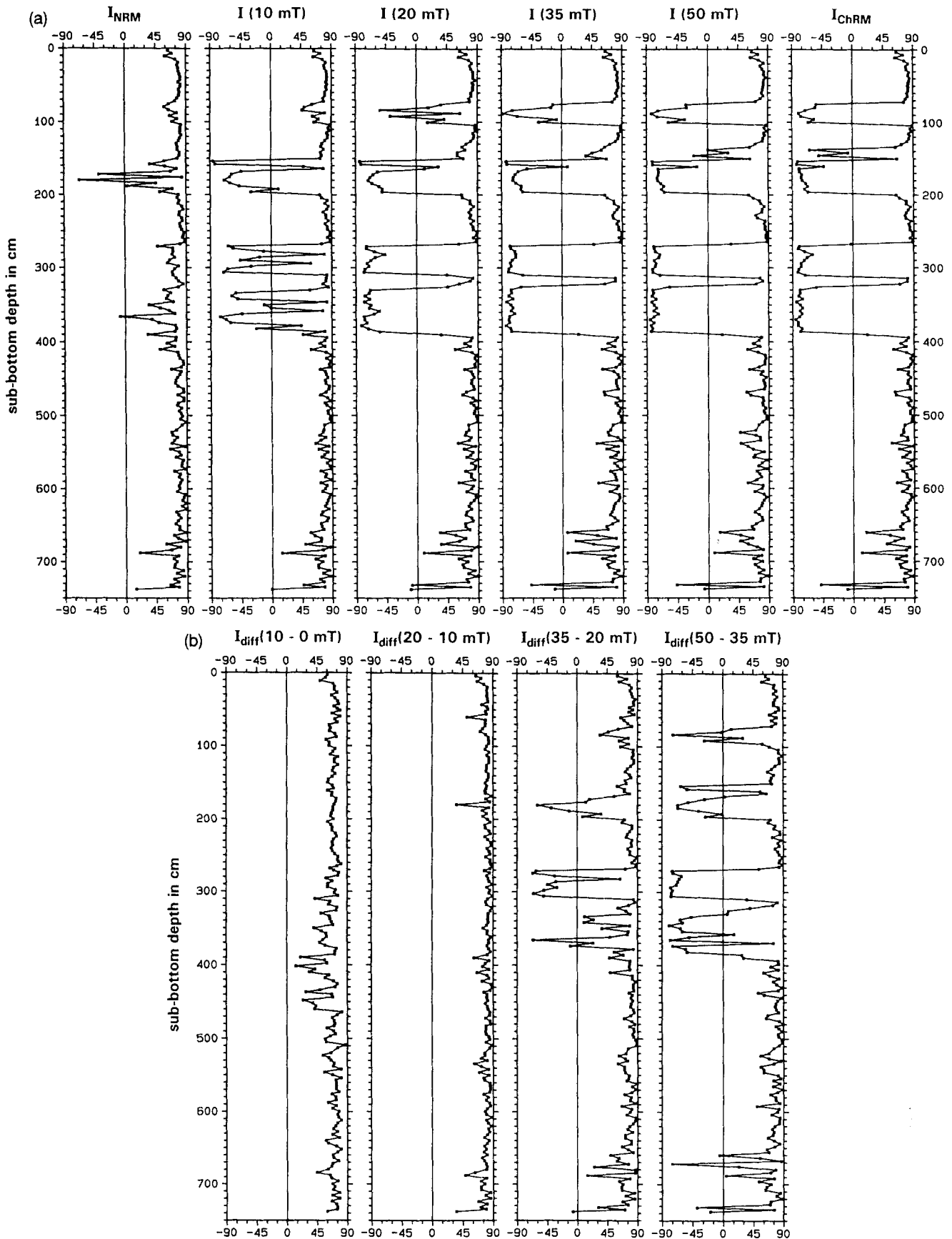


Figure 2. (a) Inclination data (I) for PS 2212-3 KAL showing the natural remanent magnetization, NRM (left), the first four demagnetization steps (middle), and the characteristic remanent magnetization, ChRM (right) as a function of sub-bottom depth; (b) the corresponding downcore variation of inclination of the difference vectors of the first four demagnetization steps displayed in (a) of the same core.

The demagnetization above 50 mT was carried out with different schemes: 70 and 100 mT for normal polarity samples and 65, 80 and 100 mT for reverse polarity samples with additional steps of 130, 160 and 200 mT where necessary in order to obtain a more detailed record of the directional variations in the course of the AF treatment.

The NRM shows typical inclinations of $+70^\circ$ to $+90^\circ$, which correspond to a site latitude of 82°N . Only the intervals between 150 and 200 cm and between 320 and 410 cm exhibit shallow to negative NRM inclinations. However, during the AF treatment, four well-defined intervals of almost ideal reverse inclinations of -70° to -90° were revealed in the upper 400 cm of the core. Within the lowermost 100 cm a few samples exhibit intermediate to reverse inclinations. Although the resultant vectors already show four intervals of intermediate to reverse inclinations after 20 mT demagnetization, the difference vectors (e.g. the remanence components destroyed during these steps) exhibit steep positive inclinations (I_{diff}) throughout the whole core (Fig. 2b). It is interesting to note that $I_{\text{diff}}(20\text{--}10\text{ mT})$ is in general much steeper than $I_{\text{diff}}(10\text{--}0\text{ mT})$, even in intervals with a reverse ChRM inclination (right column in Fig. 2a). This is interpreted as being due to a randomly oriented post-sampling viscous overprint of the remanence component removed in the first demagnetization step, whereas the steep inclination of the remanence component removed by the second demagnetization step reflects the low coercive overprint by the recent normal polarity period of the geomagnetic field only. In addition, the steep positive inclinations of the first two difference vectors are strong indicators that each sample has been taken in a correct orientation.

The next two demagnetization steps of 35 and 50 mT cause only small directional changes in the resultant vectors, especially in the two reverse inclination intervals between 265 and 390 cm (Fig. 2a). The corresponding inclination logs of the difference vectors $I_{\text{diff}}(35\text{--}20\text{ mT})$ and $I_{\text{diff}}(50\text{--}35\text{ mT})$ in Fig. 2(b) clearly demonstrate that a high-coercive reverse remanence component is being removed. However, these logs in parts still show intermediate directions whereas the resultant vectors exhibit a full reversed inclination over several demagnetization steps. This means that the remaining remanence is still partially built up by a portion of the normal overprint. The AF treatment therefore had to be extended to at least 100 mT in order to isolate a single-component ChRM separated from this overprint.

The final result of the demagnetization study of core PS 2212-3 KAL is given by the downcore variations of the ChRM inclinations in Fig. 2(a), which is an almost perfect rectangular function of the four polarity events documented in the upper half of the core. Most of the polarity reversals are completed within a depth interval covered only by two or three samples (4–8 cm). Similar results were obtained for late Quaternary sediments recovered in the Fram Strait (Nowaczyk 1991; Nowaczyk & Baumann 1992).

In the lowermost part of the core two samples with shallow and steep negative inclinations separated by a normal polarity sample can be interpreted as the top of a fifth event followed by an excursion reaching only shallow positive inclinations between 660 and 690 cm sub-bottom depth. ChRM inclinations and declinations together with the NRM intensities of core PS 2212-3 KAL are given in Fig. 3.

The ChRM declinations in the upper section of the core exhibit shifts of about 180° associated with polarity changes. However, the downcore variation of ChRM declinations of the whole core reflects the typical situation of the geomagnetic field at northern high latitudes. Because of the variable position of the magnetic North Pole, the declinations are widely scattered and reach southerly directions even during stable phases of normal polarity of the Earth's magnetic field.

MAGNETIC SUSCEPTIBILITY

Measurements of magnetic volume susceptibility were done with a Bartington M.S.2 instrument, applying two different sensors. The sensitivity depends on the integration time used for the measurement. In the fast but less precise mode, one reading can be taken in less than 1 s and the result is given in integer multiples of 10^{-5} (SI, uncalibrated). In the slower, high-precision mode a measurement takes 10 s, and the result is given in multiples of 0.1×10^{-5} (SI, uncalibrated).

For core PS 1533-3 SL, the magnetic susceptibility was determined on the palaeomagnetic samples ($V = 6.2\text{ cm}^3$) using the Bartington M.S.2.B single-sample cavity in the high-precision mode at frequencies of 460 Hz and 4600 Hz. The values of the magnetic susceptibility given by the control unit were multiplied by a factor of 16.1 in order to correct for the smaller volume of the samples and to obtain multiples of 10^{-6} .

The susceptibility for core PS 2212-3 KAL was determined on u-channel subcores using the Bartington M.S.2.F probe. The spatial resolution along the core axis is about 12 mm (Nowaczyk, Mulitza & Thießen, in preparation). For the measurement, the sensor is lowered directly onto the sediment surface, which is covered with a thin plastic foil to prevent contamination of the sensor. The logging was done each 5 mm in the fast (lower precision) mode at a frequency of 580 Hz. An empirically determined calibration factor of 18.1 was used to yield multiples of 10^{-6} (SI).

Figure 4 gives the downcore variation of magnetic susceptibility together with the ChRM inclinations of core PS 1533-3 SL (Nowaczyk & Baumann 1992) and core PS 2212-3 KAL (this study). The discrete levels visible in the susceptibility log of core PS 2212-3 KAL are due to the low precision mode of the measurements where a scale value of one equals a step in susceptibility of 18.1×10^{-6} . The correlation lines are based on the two data sets displayed in Fig. 4 with additional information from the core descriptions and the variations of the sediment colour. High values of magnetic susceptibility in general are associated with brownish sediments composed of silty clay; intervals of low susceptibility represent dark greyish sandy silt.

The most striking result in Fig. 4 is the enhancement of the spatial resolution of the magnetic susceptibility achieved by the Bartington M.S.2.F probe for core PS 2212-3 KAL (200 data points per metre) in comparison to the log based on the palaeomagnetic samples obtained with the M.S.2.B sensor for core PS 1533-3 SL (20 data points per metre). Nevertheless, the main features of the susceptibility logs are more or less the same. A more detailed discussion and interpretation of the correlation is given below.

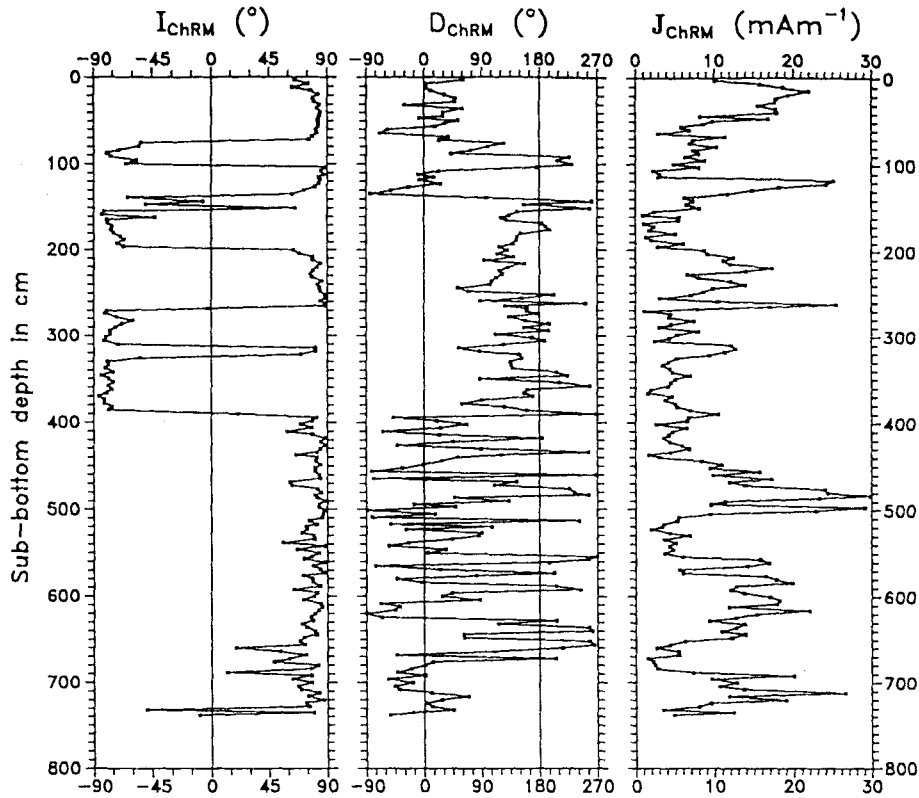


Figure 3. Core PS 2212-3 KAL: downcore variation of ChRM inclination, ChRM declination and NRM intensity.

ROCK MAGNETIC INVESTIGATIONS

Rock magnetic data were obtained from every second palaeomagnetic sample to provide information on concentration and mineralogy of ferromagnetic minerals in the sediment. When there were strong deviations from one sample to the next, the sample between was also studied. 65 samples of core PS 1533-3 SL and 110 samples of core PS 2212-3 KAL were subjected to the following non-destructive magnetic measurements.

(1) Low-field susceptibility logs κ_{lf} and frequency dependence of susceptibility κ_{fd} were obtained with the Bartington susceptibility meter in connection with the single sample cavity (M.S.2.B). Two measurements at a low frequency of 460 Hz (κ_{lf}) and a high frequency of 4600 Hz (κ_{hf}) lead to the ratio

$$\kappa_{fd} = \frac{(\kappa_{lf} - \kappa_{hf})}{\kappa_{lf}},$$

which indicates ferrimagnetic particles in the superparamagnetic/stable single-domain grain size range.

(2) Anhyseretic remanent magnetization (ARM) was acquired in a peak alternating field of 100 mT with a superimposed steady field of $B_{st} = 0.04$ mT (Earth's magnetic field). Anhyseretic susceptibility κ_{ARM} is given by the ratio ARM/B_{st} . All magnetization measurements were done with a Molspin fluxgate magnetometer (noise level $0.2 \times 10^{-3} \text{ Am}^{-1}$).

(3) Stepwise isothermal remanent magnetization (IRM)

was acquired in fields up to 800 mT. The maximum magnetization will be referred to as 'saturation' isothermal remanence (SIRM). It is quite obvious, however, that the anti-ferromagnetic components of the magnetic particles will not be completely saturated in this maximum field. Subsequently, the SIRM was progressively demagnetized in alternating fields of up to 150 mT (single-axis 2G Enterprises demagnetizer) to determine the median destructive field (MDF_{SIRM}). The intersection point of the acquisition and demagnetization curve projected onto the field-axis (B_{cr}^*) approximates the remanent coercivity (B_{cr}) (Cisowski 1981).

(4) In order to detect high-coercivity phases, the samples were magnetized again in a d.c. field of 800 mT followed by a backfield of 300 mT. The resulting positive component of the remanence should be due only to high-coercive anti-ferromagnetic minerals, because even the hardest ferrimagnetic particles would be remagnetized in a field of 300 mT. These two remanence measurements were used to calculate

$$S_{-0.3T} = \frac{1}{2} \left(1 - \frac{IRM_{-0.3T}}{SIRM} \right),$$

which describes the change from pure haematite ($S_{-0.3T} = 0$) to pure magnetite ($S_{-0.3T} = 1$), (Bloemendal *et al.* 1992).

(5) Coercivity B_c and the ratio of remanent saturation magnetization M_{rs} to saturation magnetization M_s were derived from hysteresis loop measurements performed on 11 samples of core PS 1533-3 SL and 12 samples of core PS 2212-3 KAL. Remanence coercivity B_{cr} was determined

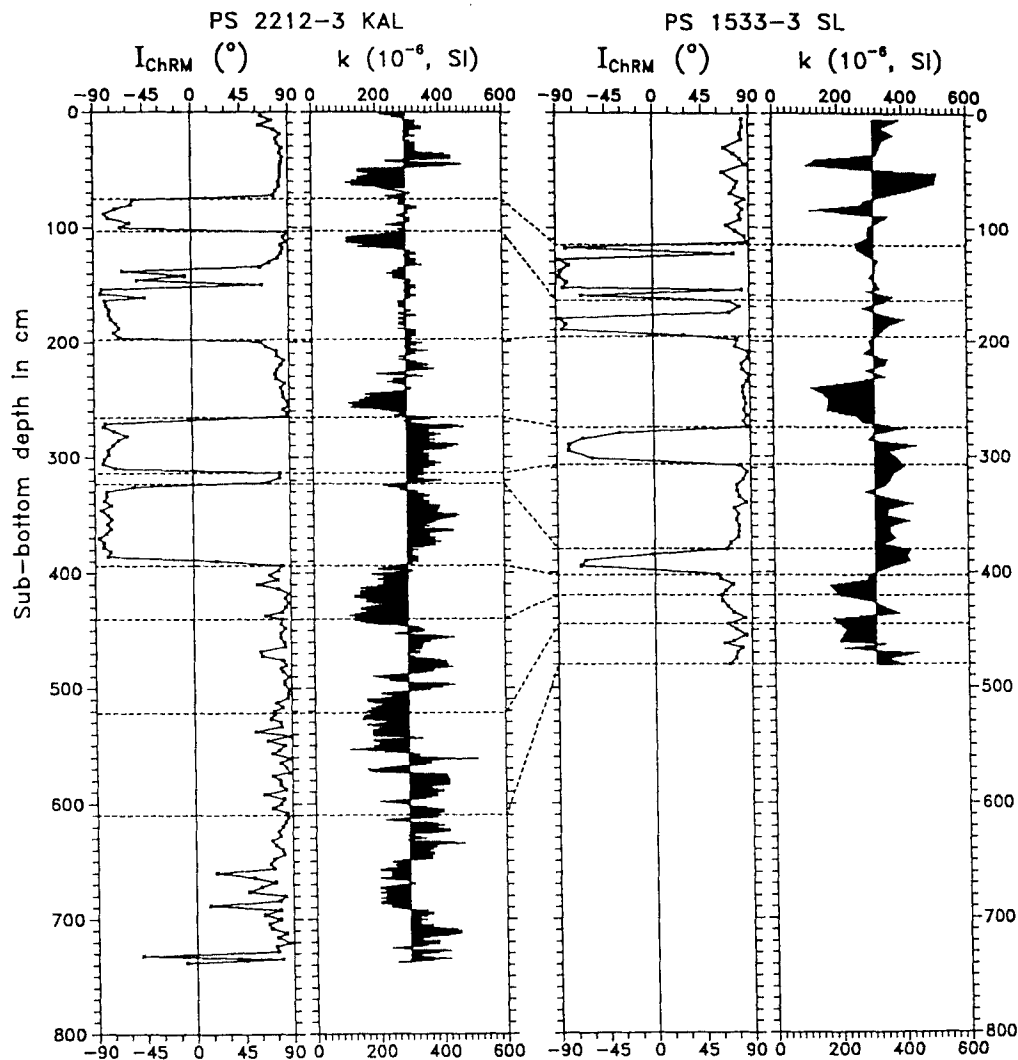


Figure 4. Correlation of cores PS 2212-3 KAL and PS 1533-3 SL based on ChRM inclination, magnetic susceptibility, and core description. Variations of the susceptibility from the total mean value are shaded in black. Dashed lines indicate horizons of identical age.

from backfield curves of the saturated samples. These measurements were done with a Micromag 2900 Alternating Gradient Field Magnetometer (AGFM) of Princeton Measurements Corporation with maximum fields of 1 T (sensitivity $1 \mu\text{Am}^2$). The hysteresis parameters give an indication of the domain status of ferrimagnetic particles.

The results of the rock magnetic investigations are presented in Figs 5 and 6. SIRM intensities are in the range of $0.4\text{--}7.1 \text{ Am}^{-1}$ for core PS 1533-3 SL and $0.9\text{--}10.9 \text{ Am}^{-1}$ for core PS 2212-3 KAL. Their downcore variations are similar to that of the low-field susceptibility κ_{lf} with values between 110×10^{-6} and 488×10^{-6} (SI) in core PS 1533-3 SL and between 111×10^{-6} and 514×10^{-6} (SI) in core PS 2212-3 KAL. IRM investigations revealed that in fields of up to 300 mT most of the samples acquired a saturation of more than 95 per cent of the SIRM, indicating that magnetite is the principal magnetic mineral. An increase of remanence in stronger fields is caused by high-coercivity magnetic minerals like haematite or goethite. Normalized IRM acquisition and demagnetization curves of eight samples,

four from each core, are presented in Fig. 7. We chose two samples with a normal ChRM polarity and two samples with a reversed ChRM polarity, one with lower and the other with higher coercivity for each core.

We interpret the results in Fig. 7 to indicate that recorded polarity events do not correlate with changes of rock magnetic properties of the samples. The normalized IRM curves of normal and reversed samples of the same 'coercivity class' are nearly identical. Therefore, it can be assumed that normal and reversed ChRM polarity is carried by the same assemblage of magnetic grains.

The ratio SIRM/κ_{lf} is largely independent of concentration and is dependent on grain size or domain status, if magnetite is the dominant magnetic mineral (Thompson & Oldfield 1986). SIRM/κ_{lf} values from 4 to 28 kAm^{-1} (Tables 3 and 4) correspond to fine-grained magnetite of an average grain size of 0.10 to $0.22 \mu\text{m}$ (Dunlop 1986). The ratio would increase and indicate smaller particles if the paramagnetic susceptibility of the clay fraction of the sediment were to be subtracted.

The downcore variations of ARM intensities are mostly

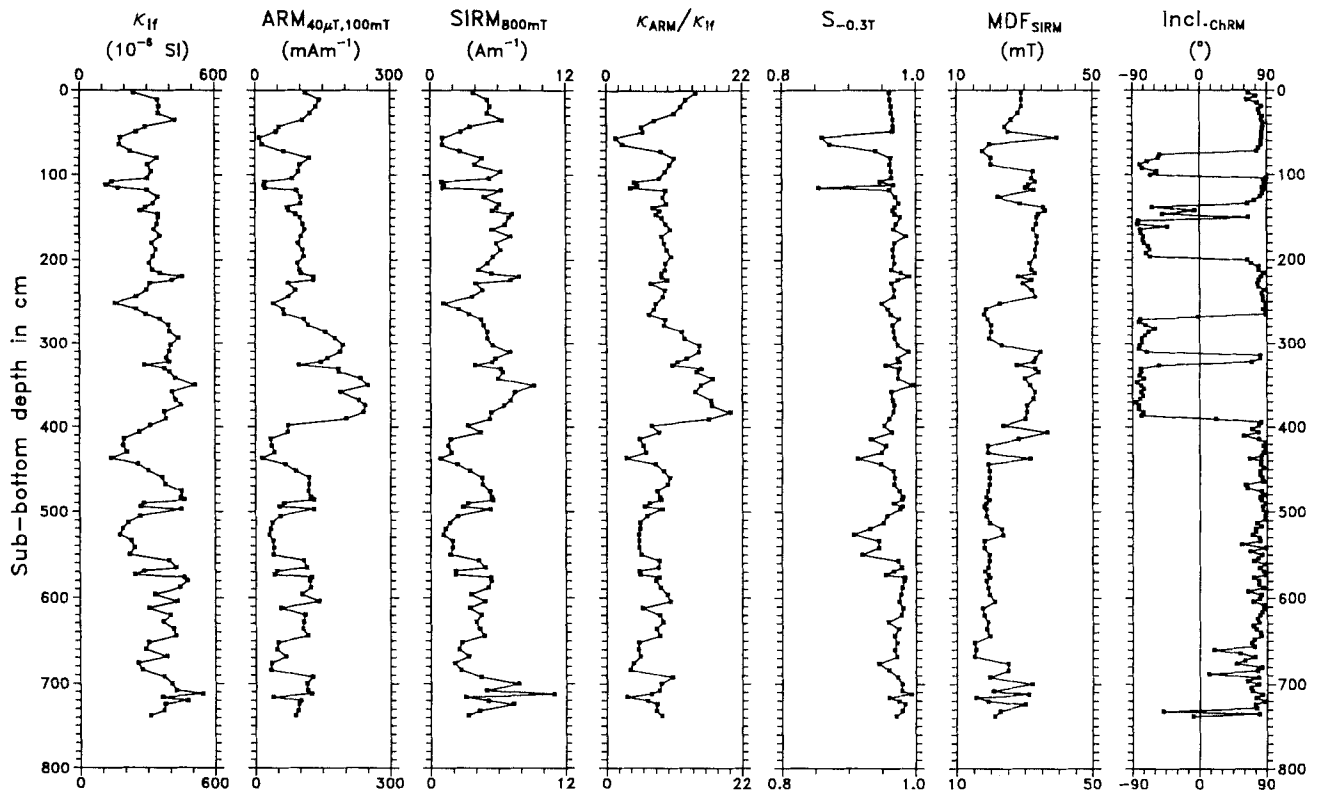


Figure 5. Downcore variations of rock magnetic parameters of core PS 2212-3 KAL. For an explanation of rock magnetic parameters, see Table 3.

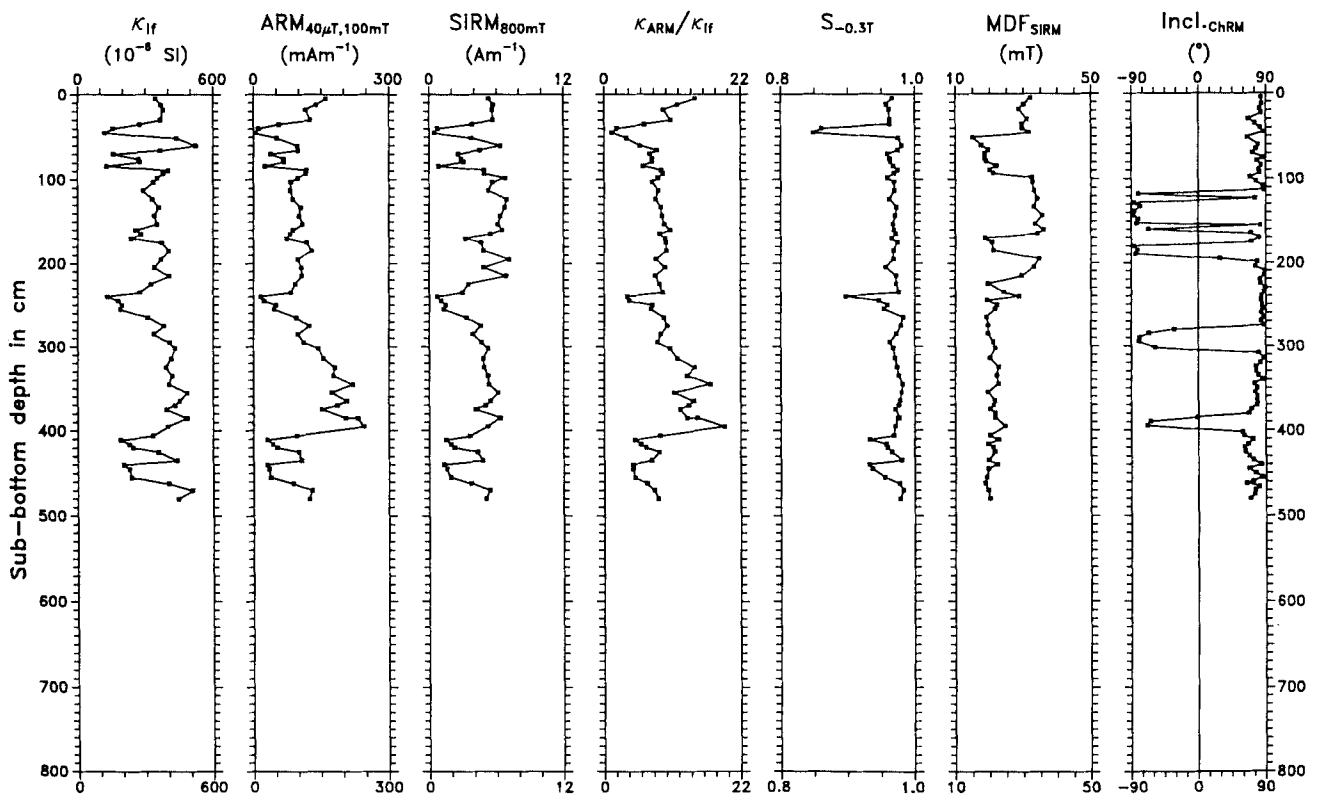


Figure 6. Downcore variations of rock magnetic parameters of core PS 1533-3 SL. For an explanation of rock magnetic parameters, see Table 3.

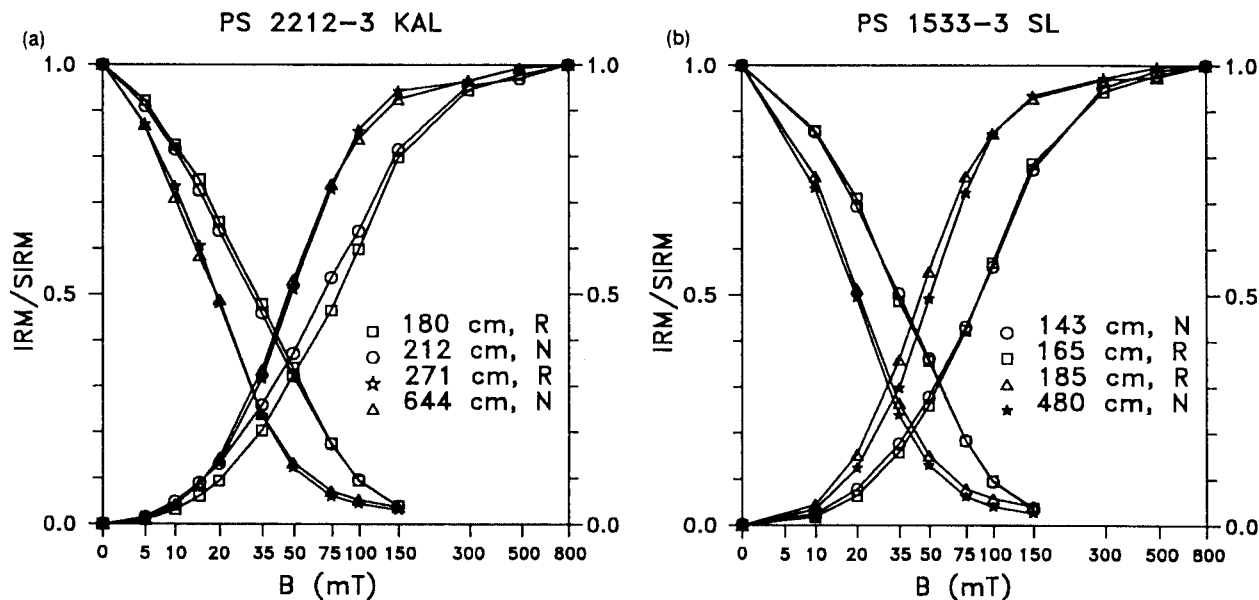


Figure 7. Normalized IRM acquisition and alternating field demagnetization curves of four typical samples of (a) core PS 2212-3 KAL and (b) core PS 1533-3 SL. N denotes a normal and R a reversed ChRM polarity.

similar to those of SIRM and κ_{lf} (Figs 5 and 6) with intensities from about 5 to 250 mA m^{-1} .

The ratio of anhysteretic susceptibility to low-field susceptibility κ_{ARM}/κ_{lf} is also indicative of grain size, because the trend of each parameter is opposite with increasing grain size. High ratios stand for fine particles and

low ratios represent coarse particles. κ_{ARM}/κ_{lf} was first introduced by King *et al.* (1982) and it is frequently used for characterizing the grain size of assemblages of magnetite particles (Hall & King 1989; Bloemendal *et al.* 1992). κ_{ARM}/κ_{lf} with values between about 1 and 20 (mean 9) compare to magnetite grain sizes of about 0.1 μm

Table 3. Rock magnetic parameters of representative samples of core PS 2212-3 KAL.

Depth	κ_{lf}	ARM	SIRM	ARM/ κ_{lf}	IRM/ κ_{lf}	ARM/ IRM	κ_{fd}	$\kappa_{ARM}/$ κ_{lf}	$S_{-0.3T}$	MDF_{IRM}	B_{cr}^*	B_{cr}	B_c	B_{cr}/B_c	M_{rs}/M_s
[cm]	[10^{-6}SI]	[Am^{-1}]	[mA m^{-1}]	[kAm^{-1}]	[kAm^{-1}]					[mT]	[mT]	[mT]	[mT]		
11	340	143	5.1	0.42	14.9	0.03	0.07	13	0.96	29.0	40.5	48.4	17.8	2.719	0.233
56	171	9	1.1	0.05	6.2	0.01	0.01	2	0.86	39.5	52.5	45.4	11.6	3.914	0.160
115	166	21	1.1	0.13	6.3	0.02	0.03	4	0.86	30.0	44.5	50.4	15.4	3.273	0.186
180	314	94	5.8	0.30	18.5	0.02	0.08	9	0.97	33.5	51.0	62.9	25.0	2.516	0.286
252	153	40	1.1	0.26	7.4	0.04	0.04	8	0.95	22.5	35.0	47.0	19.3	2.435	0.189
271	349	108	4.5	0.31	12.9	0.02	0.03	10	0.98	19.0	32.0	36.3	16.3	2.227	0.200
358	403	188	7.5	0.47	18.6	0.03	0.06	15	0.97	33.0	47.0	55.0	23.7	2.321	0.304
437	135	14	0.9	0.10	6.4	0.02	0.01	3	0.92	31.5	44.5	38.4	15.0	2.560	0.174
486	438	131	5.5	0.30	12.6	0.02	0.03	9	0.98	19.5	31.0	34.7	15.6	2.224	0.184
550	209	40	1.8	0.19	8.4	0.02	0.03	6	0.92	19.5	31.5	38.1	15.4	2.474	0.187
644	409	116	4.7	0.28	11.5	0.02	0.02	9	0.97	19.5	31.5	35.7	15.4	2.318	0.172
724	364	97	7.3	0.27	20.0	0.01	0.02	8	0.99	30.0	46.0	36.6	15.9	2.302	0.184

Depth: Sub-bottom depth of sample.

κ_{lf} : Low-field susceptibility at 460 Hz.

$\kappa_{fd} = (\kappa_{lf} - \kappa_{hf})/\kappa_{lf}$: Frequency-dependent susceptibility; low frequency 460 Hz, high frequency 4600 Hz.

κ_{ARM} : Anhysteretic susceptibility: ARM divided by the strength of d.c. field.

ARM: Anhysteretic remanent magnetization; peak AF field 100 mT, d.c. field 0.04 mT.

SIRM: Isothermal saturation remanent magnetization; d.c. field 800 mT.

$S_{-0.3T} = \frac{1}{2}(1 - [IRM_{-0.3T}/SIRM])$; $IRM_{-0.3T}$: magnetization after demagnetizing SIRM by a reversed field of 300 mT.

MDF_{SIRM} : Median destructive field of SIRM acquired in a steady field of 800 mT.

B_{cr}^* : Remanent coercivity determined after Cisowski (1981).

B_{cr} : Remanent coercivity determined by backfield method.

B_c : Coercivity determined by hysteresis experiments, corrected for high-coercive constituents.

M_{rs}/M_s : Ratio of saturation remanent magnetization and saturation magnetization, determined by hysteresis experiments, maximum d.c. field 1 T, corrected for high-coercive constituents.

Table 4. Rock magnetic parameters of representative samples of core PS 1533-3 SL. For further explanation, see Table 3.

Depth	κ_{if}	ARM	SIRM	ARM/ κ_{if}	IRM/ κ_{if}	ARM/ IRM	κ_{fd}	$\kappa_{ARM}/$ κ_{if}	$S_{-0.3T}$	MDF _{IRM}	B_{cr}^*	B_{cr}	B_c	B_c/B_c	M_{rs}/M_s
[cm]	[$10^{-6}Si$]	[Am^{-1}]	[mAm^{-1}]	[kAm^{-1}]	[kAm^{-1}]					[mT]	[mT]	[mT]	[mT]		
12	338	139	5.7	0.41	16.9	0.02	0.05	13	0.96	30.0	42.0	48.6	14.7	2.467	0.281
45	109	5	0.4	0.05	4.0	0.01	0.06	2	0.85	31.5	43.5	48.3	13.2	3.659	0.142
51	394	50	3.7	0.13	9.5	0.01	0.02	4	0.98	15.0	25.5	28.8	10.7	2.692	0.128
84	119	26	0.9	0.22	7.4	0.03	0.04	7	0.97	22.0	34.0	39.3	16.8	2.339	0.167
160	232	88	6.5	0.38	28.2	0.01	0.05	12	0.97	36.0	53.0	65.2	25.6	2.547	0.248
165	258	81	5.5	0.31	21.2	0.01	0.03	10	0.97	34.0	57.0	65.7	26.4	2.489	0.254
185	375	129	4.8	0.34	12.9	0.03	0.03	11	0.97	21.0	32.0	35.8	15.5	2.310	0.192
240	127	16	0.7	0.13	5.5	0.02	0.05	4	0.90	28.5	41.0	53.7	20.0	2.685	0.222
385	459	204	6.3	0.44	13.6	0.03	0.04	14	0.98	21.5	32.0	36.4	16.2	2.247	0.210
411	180	30	1.5	0.17	8.4	0.02	0.04	5	0.94	22.5	34.0	39.6	14.3	2.769	0.157
470	488	130	5.4	0.27	11.1	0.02	0.04	8	0.99	19.5	31.5	35.5	15.4	2.305	0.172

(Bloemendal *et al.* 1992). For calculation of κ_{ARM}/κ_{if} , the paramagnetic fraction is of great importance, because it lowers the value of κ_{ARM}/κ_{if} . The correction for the paramagnetic constituents results in inferred smaller particle sizes. The small grain sizes are in accordance with results from the Alpha Ridge (Bloemendal *et al.* 1992) and with those for synthetic submicron magnetite (Maher 1988).

The median destructive fields determined from SIRM demagnetization MDF_{SIRM} range from 15 to 40 mT. They are in good agreement with data of fine-grained magnetite (Maher 1988).

The concentration of high-coercivity anti-ferromagnetic phases could be estimated by $S_{-0.3T}$. The average $S_{-0.3T}$ for both curves is about 0.96 (Figs 5 and 6; Tables 3 and 4) indicating an amount of up to 50 per cent haematite (Bloemendal *et al.* 1992). Owing to their low saturation magnetization and the high saturating fields, the anti-ferromagnetic constituents carry only 5 per cent of the SIRM, as can be seen from the SIRM demagnetization curves (Fig. 7). Only in a few samples do anti-ferromagnetic minerals contribute to SIRM by up to 15 per cent.

Other rock magnetic parameters as derived from hysteresis loop and backfield curve measurements as well as the determination of B_{cr}^* give evidence that small titanomagnetite particles dominate the remanence in the sediments studied.

In summary, at both sites the rock magnetic parameters are very similar, indicating an identical magnetomineralogy with fine-grained titanomagnetite as the carrier mineral.

DATING OF THE CORES

There are several different datings available for the cores discussed in this paper. AMS-¹⁴C datings of four depth levels and a $\delta^{18}O$ stratigraphy for core PS 1533-3 SL are given by Köhler (1991, Table 2). Unfortunately the oxygen isotope data are incomplete due to the lack of foraminifera. However, additional geochronologic information for this core is provided by a ¹⁰Be and ²³⁰Th stratigraphy in this study (see also Hentzschel 1992). Both cores have been investigated for calcareous nannofossils. The nannofossil data of core PS 1533-3 SL have already been published by Nowaczyk & Baumann (1992). The new core from the

Yermak Plateau, PS 2212-3 KAL, has been analysed for calcareous nannofossils in this study. We discuss the new ¹⁰Be and ²³⁰Th stratigraphy of core PS 1533-3 SL and the nannofossil data of core PS 2212-3 KAL.

¹⁰Be and ²³⁰Th measurements of core PS 1533-3 SL

Sampling of core PS 1533-3 SL for ¹⁰Be measurements was done integrating over 10 cm intervals and for ²³⁰Th measurements integrating over 5 cm intervals. The chemical preparation of these samples follows the procedure described by Henken-Mellies *et al.* (1990) and Anderson (1982). The ¹⁰Be measurements were performed at the AMS (accelerated mass spectrometry) facility at the ETH Zürich, Switzerland. The ²³⁰Th measurements were performed at the Institut für Umweltphysik in Heidelberg, Germany.

The ¹⁰Be and decay corrected ²³⁰Th_{ex} concentrations of core PS 1533-3 SL are presented as a function of sub-bottom depth (Fig. 8). The main purpose of the ¹⁰Be and ²³⁰Th data in this study is for stratigraphic dating of core PS 1533-3 SL only. A more detailed description of these measurements and interpretation of the results will be presented elsewhere (Eisenhauer *et al.*, 1994).

In previous publications, comparison of high-resolution ¹⁰Be and ²³⁰Th data to the corresponding $\delta^{18}O$ records showed that there is a link between ¹⁰Be and ²³⁰Th concentrations and palaeoclimate. High ¹⁰Be concentrations in sediments from high latitudes are attributed to interglacial periods and low ¹⁰Be concentrations are attributed to glacial stages. Climatic transitions in these cores are marked by drastic changes of isotope concentrations (Eisenhauer *et al.* 1990, 1991). Similar to the $\delta^{18}O$ stratigraphy, this '¹⁰Be and ²³⁰Th stratigraphy' can be used as an independent stratigraphic tool for dating sediment cores from northern high latitudes. In particular, the application of this method is of special interest for such sediment cores where the application of the $\delta^{18}O$ method is restricted due to small amounts or the complete lack of carbonate (foraminiferas) as well as the influence of isotopically light meltwater.

Here we present the chronology of core PS 1533-3 SL which is based on the ¹⁰Be and ²³⁰Th stratigraphy and on $\delta^{18}O$ stratigraphy (Köhler 1991). In Fig. 8, horizontal

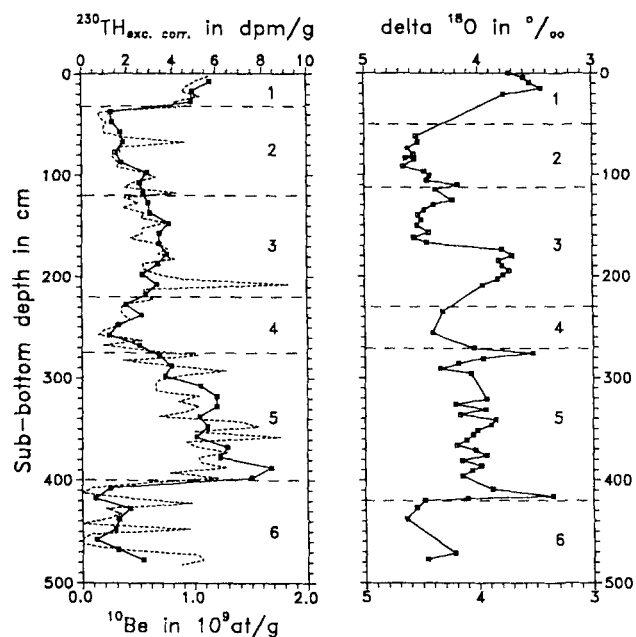


Figure 8. Core PS 1533-3 SL: downcore variations of ^{10}Be (—■—) and decay corrected $^{230}\text{Th}_{\text{ex}}$ concentrations (----) and $\delta^{18}\text{O}$ stratigraphy by Köhler (1991). Numbers along the right margins of each plot denote oxygen isotope stages 1 through 6 with their boundaries indicated by horizontal dashed lines.

dashed lines indicate drastic changes of the ^{10}Be and ^{230}Th concentrations attributed to climatic transitions according to the SPECMAP time scale (Imbrie *et al.* 1984). For comparison in the $\delta^{18}\text{O}$ record, we also marked those sub-bottom depths where climatic transitions occurred according to the $\delta^{18}\text{O}$ record of this core. As seen from Fig. 8, both stratigraphic dating methods gave comparable results. However, a detailed inspection of Fig. 8 shows that the transitions of termination I and II as determined from the ^{10}Be and ^{230}Th stratigraphy are shifted upwards by about 20 cm relative to the $\delta^{18}\text{O}$ record. This may reflect the input of isotopically light meltwater during the transition from a glacial to an interglacial period which superimposed the 'climatic' signal of the $\delta^{18}\text{O}$ record of this core. In addition, the $\delta^{18}\text{O}$ record is partially incomplete; in particular, in the depth range of termination I too few foraminifera were available for $\delta^{18}\text{O}$ measurements. Therefore we argue that the ^{10}Be and ^{230}Th stratigraphy provides a more precise determination of this climatic transition than the $\delta^{18}\text{O}$ record of core PS 1533-3 SL. However, the good agreement of these independent methods provides a refined determination of sedimentation rates and hence a precise chronology for core PS 1533-3 SL.

Calcareous nannofossil biostratigraphy

Core PS 2212-3 KAL

The topmost 732 cm of core PS 2212-3 KAL was sampled for calcareous nannofossils (coccoliths) at about 5–10 cm intervals. Smear slides were prepared from the raw sediment and studied in a light microscope at 1250 \times magnification. The numbers of different taxa of nannofossils in 20 fields of

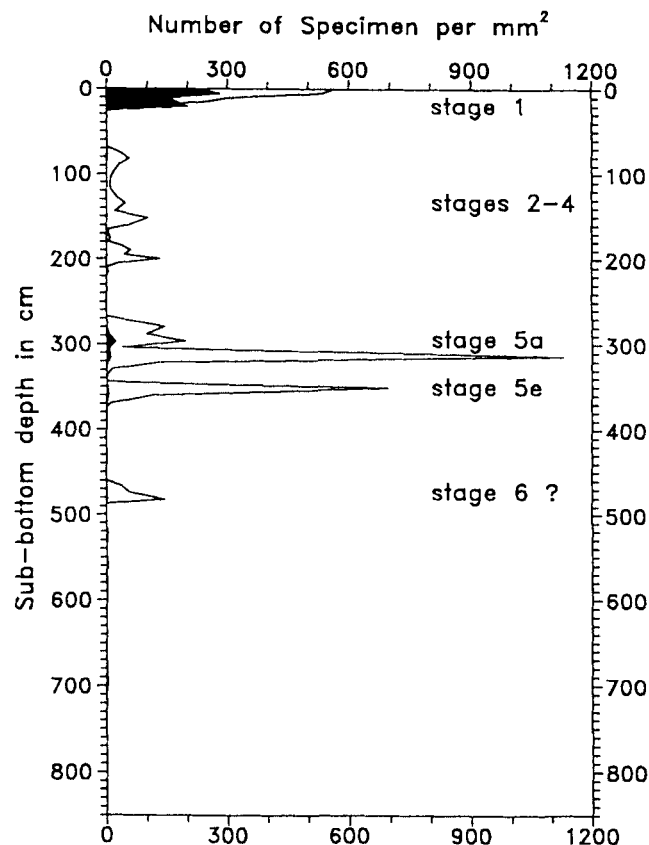


Figure 9. Core PS 2212-3 KAL: abundances of small placoliths, *Emiliana huxleyi* and *Gephyrocapsa* spp. (solid line), and *Coccolithus pelagicus* (black) and approximate levels of oxygen isotope stages 1 through 6.

view were recorded. The abundance is expressed as numbers of specimens per mm^2 in the smear slides—a technique described by Backman & Shackleton (1983).

The numbers of nannofossils vary strongly at different levels of core PS 2212-3 KAL and nannofossils are totally absent at some levels (Fig. 9). The assemblage is dominated by small placoliths: *Gephyrocapsa* spp. and *Emiliana huxleyi* (Lohmann) Hay & Mohler. Also common are *Coccolithus pelagicus* (Wallich) Schiller and *Calcidiscus leptoporus* (Murray & Blackman) Loeblich & Tappan, and specimens of *Helicosphaera carteri* (Wallich) Kamptner and *Syracosphaera pulchra* Lohmann are occasionally present. In addition, obviously reworked Cretaceous and Tertiary specimens are observed in many samples. This assemblage is typical for relatively warm intervals of the late Quaternary European Arctic (Nowaczyk & Baumann 1992; Gard 1993).

Total abundances and relative abundances between different species closely follow the nannofossil biozonation scheme for the European high latitudes by Gard (1988). This biozonation scheme correlates typical nannofossil assemblages in the Norwegian and Greenland seas to the oxygen isotope stratigraphy for the last 500 000 years. Little is known about the time-transgressive differences of the nannofossil assemblages between the cores dated by oxygen isotope stratigraphy in the Norwegian and Greenland seas and cores collected from the Yermak Plateau. The presence of a specific nannofossil assemblage in sediments from the

Yermak Plateau is a mere indication of the period (interglacial oxygen isotope stages) in which the sediment was deposited. It does not represent an absolute age within each oxygen isotope stage and does not delimit the extent of the isotope stage. However, because the nannofloras of the Yermak Plateau are brought in from the Norwegian and Greenland seas by the Norwegian–West Spitsbergen current system, it is possible to accurately recognize certain oxygen isotope stages through their typical nannofloral assemblage.

The topmost nannofossil-rich interval in core PS 2212-3 KAL, down to 20 cm depth, is deposited within isotope stage 1 (Fig. 9). This is indicated by the high abundances of *E. huxleyi* and *C. pelagicus*. Barren samples and low abundances of nannofossils between 25 and 267 cm represent the relatively colder interval of oxygen isotope stages 2–4. Possibly, nannofossils present around the 100–200 cm interval indicate temporary warm-water incursions during isotope stage 3. High abundances of nannofossils, dominated by *Gephyrocapsa* spp., occur between 272 and 360 cm depths. This interval approximates the relatively warm oxygen isotope stage 5. *Coccolithus pelagicus* forms a secondary abundance peak around 296 cm depth, which is indicative of substage 5a. Increased abundances of *C. leptoporus* are noted in the samples from 351 and 360 cm depths, showing substage 5e. Supporting evidence is that total abundances of nannofossils are higher in substage 5a than in substage 5e, which is typical (Gard 1988). The samples analysed below 360 cm are mostly barren of nannofossils or contain only very few, poorly preserved specimens. They probably represent the glacial conditions of isotope stage 6, when coccolithophorids were hardly able to live in the area. In the Norwegian and Greenland seas, high abundances of nannofossils are not encountered until sediments deposited during oxygen isotope stages 9 or 11 (Bleil & Gard 1989) and it is not known if these ever reached the Yermak Plateau. Thus it is not possible to delimit the maximum age of core PS 2212-3 KAL by calcareous nannofossils.

Core PS 1533-3 SL

A combined high-resolution magnetostatigraphy and nannofossil biostratigraphy of core PS 1533-3 SL (Nowaczyk & Baumann 1992) yielded an age of about 170 Ka (lower oxygen isotope stage 6) for the end of this core. Sedimentation of *Coccolithus pelagicus* indicate Holocene age (<10 Ka) for the upper 20 cm. The dominance of the flora by *Gephyrocapsa* spp. between 285 and 360 cm represent sedimentation within stage 5. The abundance of *Emiliania huxleyi* from 60 to 120 cm is interpreted by Nowaczyk & Baumann (1992) to represent stage 3 sediments.

CHRONO-MAGNETOSTRATIGRAPHIC RESULTS

The chronostratigraphic time-frame provided by AMS-¹⁴C, $\delta^{18}\text{O}$, and ¹⁰Be/²³⁰Th data available for core PS 1533-3 SL is summarized in Table 2. From these data and the correlation given in Fig. 4, it can be concluded that the sediments recovered at sites PS 1533 and PS 2212 are not older than about 170 Ka. Intervals of negative inclination therefore are

interpreted as records of geomagnetic polarity events within the Brunhes Chron. A compilation of published palaeomagnetic excursions with inferred ages of less than 500 Ka is shown in Table 5.

The chronostratigraphic interpretation of core PS 1533-3 SL previously presented by Nowaczyk & Baumann (1992) has to be revised for the upper 200 cm (Table 2). In this core, four major intervals of negative inclinations are documented (Fig. 4). Nowaczyk & Baumann (1992) related the complex inclination variations between 115 and 195 cm to the Laschamp event (Bonhommet & Babkine 1967; Table 5). From the AMS-¹⁴C age of 22.8 Ka at 110–111 cm almost directly above this depth interval (Table 2), and the correlation with core PS 2212-3 KAL (Fig. 4), it is now proposed that this interval includes both the Mono Lake event (Denham & Cox 1971; Table 5) and the Laschamp event. The short documentation of the quite long Laschamp event compared to data from the Fram Strait area (Nowaczyk & Baumann 1992) at site PS 1533 is possibly due to lower sedimentation rates. There is no evidence for any hiatus cutting off the upper part of the Laschamp event. Using the age range of 34–43 Ka for the Laschamp event given by Nowaczyk & Baumann (1992) and the AMS-¹⁴C dating, an age range of 24–29 Ka can be calculated by linear interpolation for the Mono Lake event. This age determination is also consistent with the coccolith data of PS 2212-3 KAL which positions these two events within the time interval of oxygen isotope stages 2–4 (cf. Figs 3 and 10).

In both cores, two polarity events with negative inclinations are documented in stage 5 sediments (cf. Figs 4, 9 and 10): The Norwegian–Greenland Sea event (Bleil & Gard 1989, Table 5) within the late oxygen isotope stage 5, and the Blake event (Smith & Foster 1969; Table 5) within the early stage 5. The ages of these two events were determined by linear interpolation between the beginning and end of oxygen isotope stage 5 and the corresponding depth levels in core PS 1533-3 SL, averaging the ¹⁰Be/²³⁰Th and the $\delta^{18}\text{O}$ dating for oxygen isotope stage boundary 4/5 and using only the ¹⁰Be/²³⁰Th dating for boundary 5/6 since the light $\delta^{18}\text{O}$ peak around 410 cm is interpreted as a meltwater signal at the end of stage 6 (Eisenhauer *et al.* 1994). The age ranges derived in this way are 72–86 Ka for the Norwegian–Greenland Sea event and 118–128 Ka for the Blake event which accord with the age ranges compiled in Table 5.

By comparing the lithologies of both cores it can be concluded that a greyish sediment layer in core PS 1533-3 SL, which was deposited during the middle stage 5 (estimated age range, 85–115 Ka) is completely missing in core PS 2212-3 KAL.

The termination of a polarity event in the lowermost part of PS 2212-3 KAL can be related to the Biwa I event with an age range of 171–181 Ka given by Nowaczyk & Baumann (1992) based on palaeomagnetic and ¹⁰Be/²³⁰Th data for Fram Strait cores. The excursion-like shallow positive inclinations between 660 and 690 cm sub-bottom depth can then be related to an event around 150–160 Ka reported for the Baffin Bay, Alaska and Fram Strait (Table 5).

The complete age–depth relationships for core PS 1533-3 SL and core PS 2212-3 KAL are displayed in Fig. 10. The exact values of age versus depth together with the

Table 5. Ages of geomagnetic events during the last 500 Ka reported in literature. Ages in brackets [] have been revised later.

Age in Ka	Reference	Location
Postulated events younger than 20 Ka		
12.5–17.0	Clark & Kennett (1973)	Gulf of Mexico
18.0	Yaskawa <i>et al.</i> (1973)	Lake Biwa, Japan
17.0 ± 1.5	Freed & Healy (1974)	Gulf of Mexico
17.0–18.0	Noltimer & Colinvaux (1976)	Imuruk Lake, Alaska
18.0	Thouveny (1988)	Baffin Bay
Mono Lake		
24.0–24.6	Denham & Cox (1971)	Mono Lake, USA
24.0	Denham (1974)	Mono Lake, USA
24.0–25.0	Liddicoat & Coe (1979)	Mono Lake, USA
24.9–28.9	Negrini <i>et al.</i> (1984)	Summer Lake, USA
>20.0	Løvlie <i>et al.</i> (1986)	Yermak Plateau, Arctic Ocean
<30.0	Løvlie & Sandnes (1987)	Western Norway
24.0	Thouveny (1988)	Baffin Bay
25.0–31.0	Bleil & Gard (1989)	Norwegian–Greenland Sea
23.0	Levi & Karlin (1989)	Gulf of California
26.0–29.0	Levi & Karlin (1989)	Gulf of California
23.0–25.0	Nowaczyk (1991)	Fram Strait
27.0–29.0	Liddicoat (1992)	California, Nevada, USA
23.0–25.0	Nowaczyk & Baumann (1992)	Fram Strait
Lake Mungo (see Roperch, Bohommet & Levi 1988)		
25.0–30.0	Barbetti & McElhinny (1972)	Lake Mungo, Australia
35.0 ± 4.3	Huxtable & Aitken (1977)	Lake Mungo, Australia
New Zealand (Mono Lake, Laschamp ?)		
25.0–50.0	Shibuya <i>et al.</i> (1992)	Auckland Field, New Zealand
Laschamp		
—	Bonhommet & Babkine (1966)	Royat, France
[>8.0]	Bonhommet & Babkine (1967)	Laschamp, France
[8.0–20.0]	Bonhommet & Zähringer (1969)	Laschamp, France
—	Whitney <i>et al.</i> (1971)	Laschamp/Olby, France
49.0	Yaskawa <i>et al.</i> (1973)	Lake Biwa, Japan
32.0 ± 1.5	Freed & Healy (1974)	Gulf of Mexico
39.0 ± 6.0	Condomines (1978)	Olby, France
45.4 ± 2.5	Hall & York (1978)	Laschamp/Olby, France
25.8 ± 2.2	Huxtable <i>et al.</i> (1978)	Royat, France
35.0 ± 4.0	Gillot <i>et al.</i> (1979)	Laschamp, France
25.8 ± 2.2 (Lit.)	Barbetti & Flude (1979)	Royat, France
42.0 ± 5.0	Gillot <i>et al.</i> (1979)	Olby, France
32.5 ± 3.2	Guérin & Valladas (1980)	Laschamp, France
37.0 ± 3.5	Guérin & Valladas (1980)	Olby, France
[~20.0]	Kristjansson & Gudmundsson (1980)	SW Iceland
40.0–46.0	Guérin (1983)	Louchadière, France
<60.0	Løvlie <i>et al.</i> (1986)	Yermak Plateau, Arctic Ocean
<56.0	Løvlie & Sandnes (1987)	Western Norway
[10.0–30.0(Lit.)] ^a	Marshal, Chauvin & Bonhommet (1988)	Skalamaelifell, SW Iceland
33.5–50.0 (Lit.)	Roperch <i>et al.</i> (1988)	Laschamp/Olby, France
38.0–49.0	Bleil & Gard (1989)	Norwegian–Greenland Sea
41.7 ± 3.9	Chauvin <i>et al.</i> (1989)	Louchadière, France
38.0–43.0	Grünig (1991)	Weddell Sea, Antarctica
49.0–51.0	Levi & Karlin (1989)	Gulf of California
42.7 ± 7.8	Levi <i>et al.</i> (1990)	Skalamaelifell, SW Iceland
34.0–43.0	Nowaczyk & Baumann (1992)	Fram Strait; Yermak Plateau, Arctic Ocean
Norwegian–Greenland Sea		
70.0–77.0	Bleil & Gard (1989)	Norwegian–Greenland Sea
74.0–82.0	Grünig (1991)	Weddell Sea, Antarctica
65.0–77.0	Nowaczyk & Baumann (1992)	Fram Strait; Yermak Plateau, Arctic Ocean
Fram Strait		
95, 104	Thouveny <i>et al.</i> (1990)	Lac du Bouchet, France
98–102	Nowaczyk & Baumann (1992)	Fram Strait
Blake		
108.0–114.0	Smith & Foster (1969)	Caribbean; Indian Ocean; NW Atlantic
100.0–120.0	Wollin <i>et al.</i> (1971)	Caribbean; NW Pacific
104.0–117.0	Kawai <i>et al.</i> (1972)	Lake Biwa, Japan
108.0–114.0(Lit.)	Kukla & Koci (1972)	Czechoslovakia

Table 5. (Continued.)

100.0 < <i>t</i> < 125.0	Denham (1976)	NW Atlantic
100.0 < <i>t</i> < 125.0	Denham, Anderson & Bacon (1977)	NW Atlantic
~100.0	Manabe (1977)	NE Japan
105.0[-155.0]	Creer, Readman & Jacobs (1980)	Mediterranean Sea
100.0-130.0	Sasajima, Nishimura & Hirooka (1984)	Japan, Indonesia
112.0-117.0	Tucholka <i>et al.</i> (1987)	Mediterranean Sea
128.0 ± 33.0	Champion <i>et al.</i> (1988)	New Mexico, USA
131.0-138.0	Bleil & Gard (1989)	Norwegian-Greenland Sea
105.0-114.0	Herrero-Bevera <i>et al.</i> (1989)	Oregon, USA
107.0-120.0	Grünig (1991)	Weddell Sea, Antarctica
104.0-116.0	Tric <i>et al.</i> (1991b)	Mediterranean Sea
115.0-123.0	Nowaczyk & Baumann (1992)	Fram Strait; Yermak Plateau, Arctic Ocean
Baffin Bay		
129.0-161.0	Aksu (1983)	Baffin Bay, Davis Strait
[100.0-120.0] ^h	Westgate <i>et al.</i> (1985)	Alaska
149.0 ± 13.0	Westgate (1988)	Alaska
149.0 ± 13.0 (Lit.)	Gillen & Evans (1989)	Alaska
152.0-160.0	Nowaczyk & Baumann (1992)	Fram Strait
Biwa I		
175.0-190.0	Wollin <i>et al.</i> (1971)	NW Pacific
176.0-186.0	Kawai <i>et al.</i> (1972)	Lake Biwa, Japan
200.0-215.0	Ryan (1972)	Mediterranean Sea
175.0-185.0	Bleil & Gard (1989)	Norwegian-Greenland Sea
155.0 ± 47.0	Geissman <i>et al.</i> (1989)	New Mexico, USA
160.0-180.0	Liddicoat (1990)	California, USA
171.0-181.0	Nowaczyk & Baumann (1992)	Fram Strait
Biwa II		
280.0	Wollin <i>et al.</i> (1971)	NW Pacific
292.0-298.0	Kawai <i>et al.</i> (1972)	Lake Biwa, Japan
295.0-305.0	Ryan (1972)	Mediterranean Sea
260.0	Creer <i>et al.</i> (1980)	Mediterranean Sea
330.0-344.0	Bleil & Gard, (1989)	Norwegian-Greenland Sea
290.0	Grünig (1991)	Weddell Sea, Antarctica
[280.0]	Liddicoat & Bailey (1989)	California, USA
292.0-298.0 (Lit.)	Nowaczyk (1991)	Fram Strait
[252.0-262.0] ^c	Nowaczyk & Baumann (1992)	Fram Strait
Biwa III		
400.0	Wollin <i>et al.</i> (1971)	NW Pacific
350.0	Kawai <i>et al.</i> (1972)	Lake Biwa, Japan
	Kawai <i>et al.</i> (1975)	Lake Biwa, Japan
400.0	Creer <i>et al.</i> (1980)	Mediterranean Sea
400.0 (Lit.)	Nowaczyk (1991)	Fram Strait
Emperor		
460.0	Ryan (1972)	Caribbean
490.0 ± 50.0	Wilson & Hey (1981)	East Pacific
[460.0 ± 50.0] ^d	Champion, Dalrymple & Kuntz (1981)	Idaho, USA
474.0-483.0	Bleil & Gard (1989)	Norwegian-Greenland Sea

(Lit.) indicates that the age given in a paper is taken from literature and not determined for the material presented in the respective paper.

^a See Levi *et al.* (1990).

^b See Westgate (1988).

^c See Nowaczyk (1991).

^d See Champion *et al.* (1988).

sedimentation rates derived from them are summarized in Table 6. The significant differences in the sedimentation rates between the sites during the same time intervals can be explained by bathymetric variations between the two nearby sites. The distance between the two sites is about 11 km (Table 1) and while core PS 1533-3 SL was recovered from the top of a little seamount at a water depth of 2030 m, core PS 2212-3 KAL was taken beside this seamount at a considerably deeper water depth of 2550 m. Therefore water

currents, which should be stronger at the top of the seamount, possibly caused reduced sedimentation rates at site PS 1533.

The average sedimentation rates ranging from about 2 to 3 cm Ka⁻¹ at site PS 1533 and 3 to 8 Ka⁻¹ at site PS 2212 agree with previous results for the Eurasian Basin of Sejrup *et al.* (1984), Zahn, Markussen & Thiede (1985), Løvlie *et al.* (1986), Baumann (1990) and Nowaczyk & Baumann (1992). The calculated rates give further evidence for a late

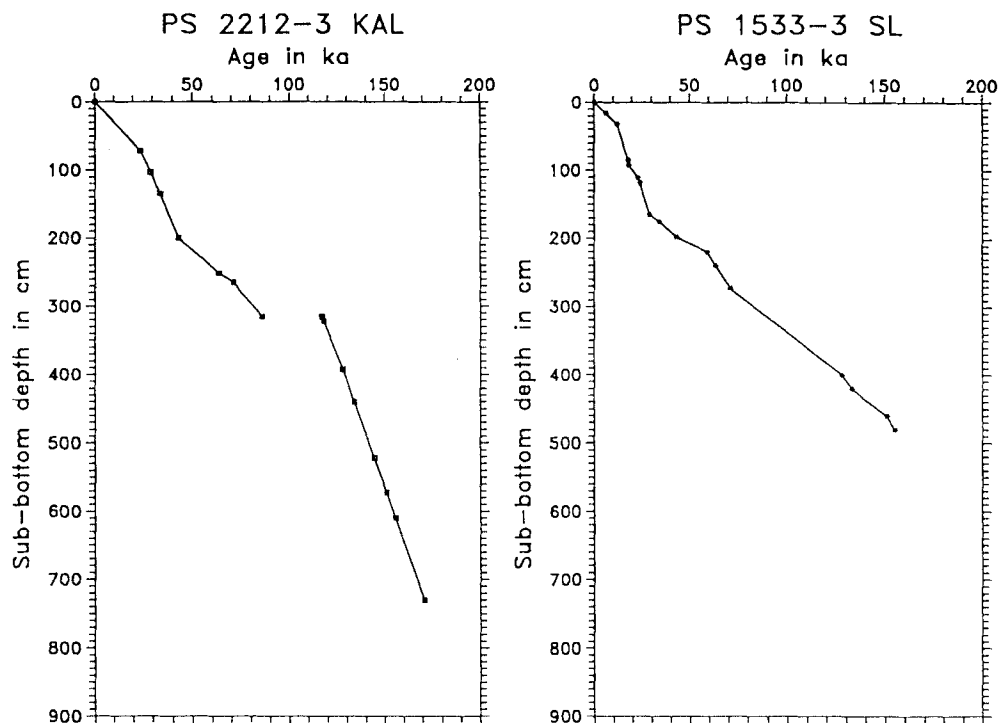


Figure 10. Age–depth relationships for cores PS 2212–3 KAL and PS 1533–3 SL derived from this study according to Table 6. For the discussion of the hiatus in core PS 2212–3 KAL, see text.

Table 6. Age–depth model and sedimentation rates for cores PS 2212–3 KAL and PS 1533–3 SL used in this study.

Depth	Age	Sedimentation rate	Depth	Age	Sedimentation rate
cm	Ka	cm Ka ⁻¹	cm	Ka	cm Ka ⁻¹
0	0		0	0	
72	24	3.0	15.5	6.165	2.5
103	29	6.2	32	12	2.8
135	34	6.4	84.5	17.87	8.9
200	43	7.2	92.5	18.16	27.6
252	63.5	2.6	110.5	22.79	3.9
265	71	1.7	118	24	6.2
315	86	3.3	165	29	9.4
----	hiatus ----	0.0	175	34	2.0
315	117		198	43	2.6
322	118	6.6	220	59	1.4
393	128	7.1	240	63.5	4.4
440	134	7.8	273	71	4.4
522	144.5	7.8	400	128	2.2
573	151	7.8	420	133	4.0
610	155	7.8	460	151	2.2
730	171	7.8	480	155	5.0

Quaternary high-deposition sedimentation environment in the Eastern Arctic Ocean. The results contrast with the low sedimentation rates in the range of only 1–2 mm Ka⁻¹ derived for the Amerasian Basin (Steuerwald, Clark & Andrew 1968; Worsley & Herman 1980; Aksu & Mudie 1985; Morris, Clark & Blasco 1985; Clark *et al.* 1986; Macko & Aksu 1986; Morris 1988; Witte & Kent 1988).

In Fig. 11 the magnetostratigraphic and susceptibility data of Fig. 4 are plotted as a function of time according to the age–depth relationships of Table 6 and Fig. 10. The gap in the inclination and susceptibility data of core PS 2212–3

KAL reflects the hiatus discussed above. The time-dependent assessment of the remanence and rock magnetic data reveals the synchronicity of the documented geomagnetic field variations (Fig. 11). Differences in older sections of the cores are due to the much higher time resolution in core PS 2212–3 KAL caused by higher sedimentation rates at this site.

In both cores four geomagnetic polarity events are clearly documented with full reversals of the ChRM inclinations. The amplitude of the inclination variations throughout the polarity events are comparable with the normal intervals of the Brunhes Chron documented in the cores (Fig. 11), except for the boundaries of the Mono Lake event and the termination of the Laschamp event documented in core PS 2212–3 KAL. Shallow negative inclinations might be associated with multipolar geometries as discussed by Chauvin, Roperch & Duncan (1990) and Clement (1991) as well as with dipolar transitional fields as discussed by Laj *et al.* (1991), Tric *et al.* (1991a) and Valet *et al.* (1992). Unfortunately, palaeo pole positions are not obtainable to test the different theories as the cores are not oriented in azimuth. The large scatter of declination at high latitudes does not allow the use of the mean ChRM declination as azimuth to re-orient the core. On the other hand, the high-resolution recording of the inferred Mono Lake event in core PS 1533–3 SL is characterized by negative inclinations typical for a dipolar direction at 82°N in the main part bounded by one normal and one full reverse sample (Figs 4 and 11). The shallow negative inclinations in core PS 2212–3 KAL therefore can also be explained by a superposition of positive and negative inclinations within one sample of the corresponding depth intervals.

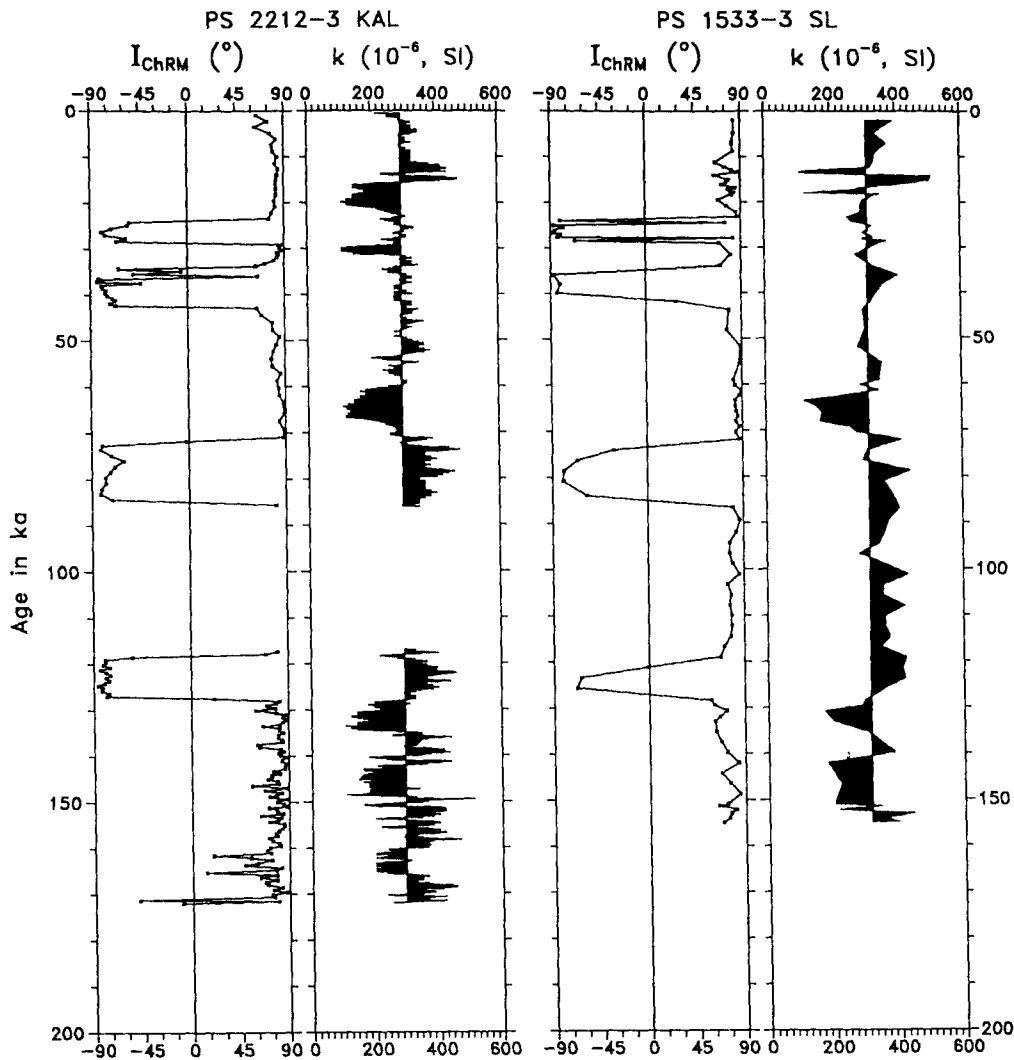


Figure 11. Magnetic susceptibility and ChRM inclination of cores PS 2212-3 KAL and PS 1533-3 SL with respect to interpreted geologic age. The data displayed in Fig. 4 have been converted into time series using the age–depth relationships of the cores given in Table 6 and Fig. 10. Display of the susceptibility data analogous to Fig. 4.

As noted, polarity transitions, especially documented by the high-quality data of core PS 2212-3 KAL, are often identified over a depth interval covered by only two or three samples, which equals 4–8 cm. This implies a time interval for the reversal process of only 0.5 to 1 Ka applying the inferred maximum sedimentation rate of 8 cm Ka^{-1} at site PS 2212. Comparable results were found for sites in the Fram Strait (Nowaczyk & Baumann 1992). The total duration of major polarity reversals derived in other studies (e.g. Opdyke, Kent & Lowrie 1973; Hillhouse & Cox 1976; Mankinen *et al.* 1985; Prévot *et al.* 1985; Clement & Kent 1991; Tric *et al.* 1991a) ranges from 5 to 10 Ka with polarity rebounds taking a time of 1 Ka. The polarity events within the Brunhes Chron recorded in the sediments of the Yermak Plateau and other sites (see Table 5) therefore might be aborted attempts of the Earth's magnetic field to reverse polarity.

CONCLUSIONS

High-quality magnetostratigraphic data were obtained for core PS 1533-3 SL and core PS 2212-3 KAL recovered from

the eastern slope of the Yermak Plateau. A detailed correlation of the cores is provided by high-resolution magnetic susceptibility data. In the downcore variations of the inclination of both cores, four geomagnetic events with full reversed polarity are documented. Several different dating methods based on AMS- ^{14}C , $\delta^{18}\text{O}$, $^{10}\text{Be}/^{230}\text{Th}$ and nannofossil data consistently yielded age ranges of 24–29 Ka for the Mono Lake event, 34–43 Ka for the Laschamp event, 72–86 Ka for the Norwegian–Greenland Sea event and 118–128 Ka for the Blake event. The termination of the Biwa I event (171–181 Ka) is inferred to lie at the bottom of core PS 2212-3 KAL.

Rock magnetic studies revealed that fine-grained titanomagnetite/titanomaghemite is the dominant magnetic phase. High-coercivity minerals (haematite/goethite) contribute to the saturation remanent magnetization usually only in the order of 5 per cent. The rock magnetic parameters indicate comparable magnetomineralogies at both sites. Downcore variations of rock magnetic parameters do not coincide with polarity changes of the ChRM.

Progressive demagnetization of core PS 2212-3 KAL samples demonstrates that events residing in the Yermak

Plateau sediments are largely affected by a normal polarity overprint, removed by alternating field demagnetization with peak amplitudes of more than 50 mT, until a high-coercivity single-component reverse polarity remanence is then isolated. However, this normal polarity overprint proves the reliability of the results, because a lot of processes can destroy the original magnetization of sediments but no conceivable post-depositional process can systematically produce a high-coercive remanence direction anti-parallel to the geomagnetic field leaving the low-coercive normal component untouched. The high-quality palaeomagnetic and chronostratigraphic data obtained in this study, as well as literature data compiled in Table 5, leave no doubt that the normal polarity of the Earth's magnetic field has been interrupted by at least four short-lived reverse polarity events during the last 170 Ka.

The duration of the transition process derived from the Yermak Plateau data can be estimated to be in the range of only 1 Ka, considerably shorter than derived for major reversals like the Matuyama–Brunhes transition, interpreted to last about 5–10 Ka. This is again equivalent to the average duration determined for the individual Brunhes Chron polarity events, so they possibly are complete but unstable reversals of the geomagnetic field.

ACKNOWLEDGMENTS

We wish to thank Professors U. Bleil, J. Thiede and G. Wefer, who supported and encouraged the work. The crews of RV *Polarstern* are acknowledged for their technical assistance during cruises ARK IV/3 and Arctic'91 (ARK VIII/3). The Alfred-Wegener-Institut für Polar- und Meeresforschung provided ship-time. We also thank Dr H. Kassens and Dr R. F. Spielhagen from GEOMAR, Kiel for collaboration on board RV *Polarstern*, and Professor R. Løvlie and Dr T. v. Dobeneck for fruitful discussions and improving the manuscript. This study was supported by the Bundesministerium für Forschung und Technologie, Projekt Framstraße and Projekt Global Change, Abbild klimatischer gesteuerter Prozesse in marinen Sedimenten der Arktis.

REFERENCES

- Aksu, A.E., 1983. Short-period geomagnetic excursion recorded in Pleistocene sediments of Baffin Bay and Davis Strait, *Geology*, **11**, 537–541.
- Aksu, A.E. & Mudie, P.J., 1985. Magnetostratigraphy and palynology demonstrate at least 4 million years of Arctic Ocean sedimentation, *Nature*, **318**, 280–283.
- Anderson, R.F., 1982. Concentration, vertical flux, and remineralization of particulate uranium in seawater, *Geochim. cosmochim. Acta*, **46**, 1293–1299.
- Backman, J. & Shackleton, N.J., 1983. Quantitative biochronology of Pliocene and early Pleistocene calcareous nannofossils from the Atlantic, Indian and Pacific oceans, *Mar. Micropaleontology*, **8**, 141–170.
- Barbetti, M. & Flude, K., 1979. Palaeomagnetic field strengths from sediments baked by lava flows of the Chaîne des Puys, France, *Nature*, **278**, 153–156.
- Barbetti, M. & McElhinny, M., 1972. Evidence of a geomagnetic excursion 30,000 yr BP, *Nature*, **239**, 327–330.
- Baumann, M., 1990. Coccoliths in sediment cores of the eastern Arctic Basin, in *Geologic History of the Polar Oceans—Arctic versus Antarctic*, pp. 437–445, eds Bleil, U. & Thiede, J., Kluwer, Dordrecht.
- Bleil, U. & Gard, G., 1989. Chronology and correlation of Quaternary magnetostratigraphy and nannofossil biostratigraphy in Norwegian–Greenland Sea sediments, *Geol. Rundschau*, **78**, 1173–1187.
- Bloemendal, J., King, J.W., Hall, F.R. & Doh, S.-J., 1992. Rock magnetism of Late Neogene and Pleistocene deep-sea sediments: Relationship to sediment source, diagenetic processes, and sediment lithology, *J. geophys. Res.*, **97**, 4361–4375.
- Bogue, S.W. & Merrill, R.T., 1992. The character of the field during geomagnetic reversals, *Ann. Rev. Earth planet. Sci.*, **20**, 181–219.
- Bonhommet, N. & Babkine, J., 1966. Sur une direction anormale du champ magnétique terrestre au cours du Quaternaire récent, *C.R. Acad. Sci. Paris*, **262**, 919–921.
- Bonhommet, N. & Babkine, J., 1967. Sur la présence d'aimantations inversées dans la Chaîne des Puys, *C.R. Acad. Sci. Paris*, **264**, 92–94.
- Bonhommet, N. & Zahringer, J., 1969. Paleomagnetism and Potassium Argon age determinations of the Laschamp geomagnetic polarity event, *Earth planet. Sci. Lett.*, **6**, 43–46.
- Champion, D.E., Dalrymple, G.B. & Kuntz, M.A., 1981. Radiometric and paleomagnetic evidence for the Emperor reversed polarity event at 0.46 ± 0.05 M.Y. in basalt lava flows from the Eastern Snake River Plain, Idaho, *Geophys. Res. Lett.*, **8**, 1055–1058.
- Champion, D.E., Lanphere, M.A. & Kuntz, M. A., 1988. Evidence for a new geomagnetic reversal from lava flows in Idaho: discussion of short polarity reversals in the Brunhes and late Matuyama Polarity Chrons, *J. geophys. Res.*, **93**, 11667–11680.
- Chauvin, A., Duncan, R.A., Bonhommet, N. & Levi, S., 1989. Paleointensity of the earth's magnetic field and K–Ar Dating of the Louchadière volcanic flow (Central France). New evidence for the Laschamp excursion, *Geophys. Res. Lett.*, **16**, 1189–1192.
- Chauvin, A., Roperch, P. & Duncan, R.A., 1990. Records of geomagnetic reversals from volcanic islands of French Polynesia 2. Paleomagnetic study of a flow sequence (1.2–0.6 Ma) from the island of Tahiti and discussion of reversal models, *J. geophys. Res.*, **95**, 2727–2752.
- Cisowski, S., 1981. Interacting vs. non-interacting single-domain behaviour in natural and synthetic samples, *Phys. Earth planet. Inter.*, **26**, 56–62.
- Clark, D.L., Andree, M., Broecker, W.S., Mix, A.C., Bonani, G., Hofmann, H.J., Morenzoni, E., Nessi, M., Suter, M. & Woelfli, W., 1986. Arctic Ocean chronology confirmed by accelerator ^{14}C dating, *Geophys. Res. Lett.*, **13**, 319–321.
- Clark, H.C. & Kennett, J.C., 1973. Paleomagnetic excursion recorded in latest Pleistocene deep-sea sediments, Gulf of Mexico, *Earth planet. Sci. Lett.*, **19**, 267–274.
- Clement, B.M., 1991. Geographical distribution of transitional VGP's: evidence for non-zonal symmetry during the Matuyama–Brunhes geomagnetic reversal, *Earth planet. Sci. Lett.*, **104**, 48–58.
- Clement, B.M. & Kent, D.V., 1991. A southern hemisphere record of the Matuyama–Brunhes polarity reversal, *Geophys. Res. Lett.*, **18**, 81–84.
- Condomines, M., 1978. Age of the Olby–Laschamp geomagnetic polarity event, *Nature*, **276**, 257–258.
- Creer, K.M., Readman, P.W. & Jacobs, A.M., 1980. Palaeomagnetic and palaeontological dating of a section at Gioia Tauro, Italy: Identification of the Blake event, *Earth planet. Sci. Lett.*, **50**, 289–300.
- Denham, C.R., 1974. Counter-clockwise motion of paleomagnetic

- directions 24,000 years ago at Mono Lake, California, *J. geomagn. Geoelect.*, **26**, 487–498.
- Denham, C.R., 1976. Blake polarity episode in two cores from the Greater Antilles Outer Ridge, *Earth planet. Sci. Lett.*, **29**, 422–434.
- Denham, C.R. & Cox, A., 1971. Evidence that the Laschamp polarity event did not occur 13300–30400 years ago, *Earth planet. Sci. Lett.*, **13**, 181–190.
- Denham, C.R., Anderson, R.F. & Bacon, M.P., 1977. Paleomagnetism and radiochemical estimates for Late Brunhes polarity episodes, *Earth planet. Sci. Lett.*, **35**, 384–397.
- Dunlop, J.D., 1986. Hysteresis properties of Magnetite and their dependence on particle size: A test of pseudo-single-domain remanence models, *J. geophys. Res.*, **91**, 9569–9584.
- Eisenhauer, A., Mangini, A., Walter, P., Beer, J., Bonani, G., Suter, M., Hofmann, H.J. & Wölfli, W., 1990. High resolution ^{230}Th and ^{10}Be stratigraphy of core 23235-2 (Fram Strait), in *Geologic History of the Polar Oceans—Arctic versus Antarctic*, pp. 475–487, eds Bleil, U. & Thiede, J., Kluwer, Dordrecht.
- Eisenhauer, A., Bonani, G., Hofmann, H.J., Mangini, A., Spielhagen, R., Suter, M., Thiede, J. & Wölfli, W., 1991. High resolution stratigraphy of Arctic sediment cores, *PSI Mag.*, **6**.
- Eisenhauer, A., Spielhagen, R. F., Frank, M., Hentschel, G., Mangini, A., Kubik, P. W., Dittrich-Hannen, B. & Billen, T., 1994. ^{10}Be records of sediment cores from high northern latitudes—implications for environmental and climatic changes, *Earth planet. Sci. Lett.*, in press.
- Eisenhauer, A., Spielhagen, R.F., Mangini, A., Kubik, P.W., Dietrich-Hannen, B., Frank, M., Hentschel, G. & Billen, T., 1994. Reconstruction of Late Quaternary particle flux and biological productivity in the Norwegian–Greenland Sea and Arctic Ocean from high-resolution ^{10}Be records *Earth planet. Sci. Lett.*, in press.
- Freed, W.K. & Healy, N., 1974. Excursions of the pleistocene geomagnetic field recorded in Gulf of Mexico sediments, *Earth planet. Sci. Lett.*, **24**, 99–104.
- Fütterer, D.K. and the ARCTIC'91 Shipboard Scientific Party, 1992. ARCTIC'91: The Expedition ARK VIII/3 of RV 'Polarstern' in 1991, *Rep. Polar Res.*, **107**.
- Gard, G., 1988. Late Quaternary calcareous nannofossil biozonation, chronology and palaeo-oceanography in areas north of the Faeroe–Iceland Ridge, *Quat. Sci. Rev.*, **7**, 65–78.
- Gard, G., 1993. Late Quaternary coccoliths at the North Pole: Evidence of icefree conditions and rapid sedimentation in the central Arctic Ocean, *Geology*, **21**, 227–230.
- Geissman, J.W., Harlan, S.S., Brown, L., Turrin, B. & McFadden, L.D., 1989. Brunhes Chron geomagnetic excursion recorded during the late Pleistocene, Albuquerque volcanoes, New Mexico, U.S.A., in *Geomagnetism and Palaeomagnetism*, pp. 123–136, eds Lowes, J.F., Collinson, D.W., Parry, J.H., Runcorn, S.K., Tozer, D.C. & Soward, A., Kluwer, Dordrecht.
- Gillen, K.P. & Evans, M.E., 1989. New geomagnetic paleosecular-variation results from the Old Crow Basin, Yukon Territory, and their use in stratigraphic correlation. *Can. J. Earth Sci.*, **26**, 2507–2511.
- Gillot, P.Y., Labeyrie, J., Laj, C., Valladas, G., Guérin, G., Poupeau, G. & Delibrias, G., 1979. Age of the Laschamp paleomagnetic excursion revisited, *Earth planet. Sci. Lett.*, **42**, 444–450.
- Grünig, S., 1991. Quartäre Sedimentationsprozesse am Kontinentaltalhang des Süd-Orkney-Plateaus im nordwestlichen Weddellmeer, Antarktis (Quaternary sedimentation processes on the continental margin of the South Orkney Plateau, NW Weddell Sea, Antarctica; English abstract), Dissertation, University of Bremen, *Rep. Polar Res.*, **75**.
- Guérin, G., 1983. La thermoluminescence des plagioclases. Méthode de datation du volcanisme. Applications au domaine volcanique français: Chaîne des Puys, Mont Dore et Cezallier, Bas Vivarais, Thèse, Paris.
- Guérin, G. & Valladas, G., 1980. Thermoluminescent dating of volcanic plagioclases, *Nature*, **286**, 697–699.
- Hall, C.M. & York, D., 1978. K–Ar and $^{40}\text{Ar}/^{39}\text{Ar}$ age of the Laschamp geomagnetic polarity reversal, *Nature*, **274**, 462–464.
- Hall, F.R. & King, J.W., 1989. Rock-magnetic stratigraphy of Site 645 (Baffin Bay) from ODP Leg 105. *Proc. Ocean Drill. Program*, **105**, 653–665.
- Hanna, R.L. & Verosub, K.L., 1989. A review of lacustrine paleomagnetic records from western North America: 0–40,000 years BP, *Phys. Earth planet. Inter.*, **56**, 76–95.
- Henken-Mellies, W.U., Beer, J., Heller, F., Hsu, K.J., Shen, C., Bonani, G., Hofmann, H.J., Suter, M. & Wölfli, W., 1990. ^{10}Be and ^{9}Be in South Atlantic DSDP Site 519: relation to geomagnetic reversals and to sediment composition, *Earth planet. Sci. Lett.*, **98**, 267–276.
- Hentschel, G., 1992. Der Transport von ^{10}Be und ^{230}Th in die Sedimente von Kern 21533, Arktischer Ozean, *Master thesis*, Inst. f. Umweltphysik, Universität Heidelberg.
- Herrero-Bevera, E., Helsley, C.E., Hammond, S.R. & Chitwood, L.A., 1989. A possible lacustrine paleomagnetic record of the Blake episode from Pringle Falls, Oregon, U.S.A., *Phys. Earth planet. Inter.*, **56**, 112–123.
- Hillhouse, J. & Cox, A., 1976. Brunhes–Matuyama polarity transition, *Earth planet. Sci. Lett.*, **29**, 51–64.
- Huxtable, J. & Aitken, M.J., 1977. Thermoluminescent dating of Lake Mungo geomagnetic polarity excursion, *Nature*, **265**, 40–41.
- Huxtable, J., Aitken, M.J. & Bonhommet, N., 1978. Thermoluminescent dating of sediment baked by lava flows of the Chaîne des Puys, *Nature*, **275**, 207–209.
- Imbrie, J., Hays, J.D., Martinson, D.G., McIntyre, A., Mix, A.C., Morley, J.J., Pisias, N.G., Prell, W.L. & Shackleton, N.J., 1984. The orbital theory of Pleistocene climate: support from a revised chronology of the marine $\delta^{18}\text{O}$ record, in *Milankovitch and Climate*, Part 1, pp. 269–305, ed. Berger, A.L., D. Reidel Publishing, Dordrecht.
- Jacobs, J.A., 1984. *Reversals of the Earth's Magnetic Field*, Adam Hilger, Bristol.
- Kawai, N., Yaskawa, K., Nakajima, T., Torii, M. & Horie, S., 1972. Oscillating geomagnetic field with a recurring reversal discovered from Lake Biwa, *Proc. Japan Acad.*, **48**, 186–190.
- Kawai, N., Nakajima, T., Tokieda, K. & Hirooka, K., 1975. Paleomagnetism and paleoclimate, *Rock magn. paleogeophys.*, Tokyo, **3**, 110–117.
- King, J.W., Banerjee, S.K., Marvin, J. & Ozdemir, O., 1982. A comparison of different magnetic methods for determining the relative grain size of magnetite in natural materials: some results from lake sediments, *Earth planet. Sci. Lett.*, **59**, 404–419.
- Köhler, S.E.I., 1991. Spätquartäre paläo-ozeanographische Entwicklung des Nordpolarmeeres und Europäischen Nordmeeres anhand von Sauerstoff- und Kohlenstoffisotopenverhältnissen der planktischen Foraminifere *Neoglobobulimina pachiderma* (sin.), *PhD thesis*, Kiel University.
- Krause, G., Meincke, J. & Thiede, J., 1989. Scientific cruise reports of Arctic expeditions ARK IV/1, 2 & 3, *Rep. Polar Res.*, **56**.
- Kristiansson, L. & Gudmundsson, L., 1980. Geomagnetic excursion in late-glacial basalt outcrops in South-Western Iceland, *Geophys. Res. Lett.*, **7**, 337–340.
- Kukla, G.J. & Kocí, A., 1972. End of the last interglacial in the Loess record, *Quat. Res.*, **2**, 374–383.
- Laj, C., Mazaud, A., Weeks, R., Fuller, M. & Herrero-Bevera, E., 1991. Geomagnetic reversal paths, *Nature*, **351**, 447.
- Levi, S. & Karlin, R., 1989. A sixty thousand year paleomagnetic record from Gulf of California sediments: secular variation,

- late Quaternary excursions and geomagnetic implications, *Earth planet. Sci. Lett.*, **92**, 219–233.
- Levi, S., Audunsson, H., Duncan, R.A., Kristjansson, L., Gillot, P.-Y. & Jacobsson, S.P., 1990. Late Pleistocene geomagnetic excursion in Icelandic lavas: confirmation of the Laschamp excursion, *Earth planet. Sci. Lett.*, **96**, 443–457.
- Liddicoat, J.C., 1990. Aborted reversal of the palaeomagnetic field in the Brunhes Normal Chron in east-central California, *Geophys. J. Int.*, **102**, 747–752.
- Liddicoat, J.C., 1992. Mono Lake excursion in Mono Basin, California, and at Carson Sink and Pyramid Lake, Nevada, *Geophys. J. Int.*, **108**, 442–452.
- Liddicoat, J.C. & Bailey, R.A., 1989. Short reversal of the palaeomagnetic field about 280,000 years ago at Long Valley, California, in *Geomagnetism and Palaeomagnetism*, pp. 137–153, eds Lowes, J.F., Collinson, D.W., Parry, J.H., Runcorn, S.K., Tozer, D.C. & Soward, A., Kluwer, Dordrecht.
- Liddicoat, J.C. & Coe, R.S., 1979. Mono Lake geomagnetic excursion, *J. geophys. Res.*, **84**, 261–271.
- Løvlie, R., 1989. Paleomagnetic stratigraphy: a correlation method, *Quat. Int.*, **1**, 129–149.
- Løvlie, R. & Sandnes, A., 1987. Paleomagnetic excursions recorded in mid-Weichselian cave sediments from Skjonghelleren, Valderøy, W. Norway, *Phys. Earth planet. Inter.*, **45**, 337–348.
- Løvlie, R., Markussen, B., Sejrup, H.P. & Thiede, J., 1986. Magnetostratigraphy in three Arctic Ocean sediment cores: arguments for geomagnetic excursions within oxygen-isotope stage 2-3, *Phys. Earth planet. Inter.*, **43**, 173–184.
- Macko, S.A. & Aksu, A.E., 1986. Amino acid epimerization in planktonic foraminifera suggests slow sedimentation rates for Alpha Ridge, Arctic Ocean, *Nature*, **322**, 730–732.
- Maher, B.A., 1988. Magnetic properties of some synthetic sub-micron magnetites, *Geophys. J.*, **94**, 83–96.
- Manabe, K.-I., 1977. Reversed magnetozone in the late Pleistocene sediments from the Pacific coast of Odaka, northeast Japan, *Quat. Res.*, **7**, 372–379.
- Mankinen, E.A., Prévot, M., Grommé, C.S. & Coe, R.S., 1985. The Steens Mountain (Oregon) geomagnetic polarity Transition 1. Directional history, duration of episodes, and rock magnetism, *J. geophys. Res.*, **90**, 10,393–10,416.
- Marshall, M., Chauvin, A. & Bonhommet, N., 1988. Preliminary paleointensity measurements and detailed magnetic analysis of basalts from the Skalamaelifell excursion, southwest Iceland, *J. geophys. Res.*, **93B**, 11 681–11 698.
- Morris, T.H., 1988. Stable isotope stratigraphy of the Arctic Ocean: Fram Strait to Central Arctic, *Palaeogeog., Palaeoclimat., Palaeoecol.*, **64**, 201–219.
- Morris, T.H., Clark, D.L. & Blasco, S.M., 1985. Sediments of the Lomonosov Ridge and Makarov Basin: a Pleistocene stratigraphy for the North Pole, *Geol. Soc. Am. Bull.*, **96**, 901–910.
- Negrini, R.M., Davis, J.O. & Verosub, K.L., 1984. Mono Lake excursion found at Summer Lake, Oregon, *Geology*, **12**, 643–646.
- Noltimer, H.C. & Colinvaux, P.A., 1976. Geomagnetic excursion from Imuruk, Alaska, *Nature*, **259**, 197–200.
- Nowaczyk, N.R., 1991. Hochauflösende Magnetostratigraphie spätquartärer Sedimente arktischer Meeresgebiete (High-resolution magnetostratigraphy of late-Quaternary Arctic marine sediments, English abstract), Dissertation, University of Bremen, *Rep. Polar Res.*, **78**.
- Nowaczyk, N.R. & Baumann, M., 1992. Combined high-resolution magnetostratigraphy and nanofossil biostratigraphy for late Quaternary Arctic Ocean Sediments, *Deep-Sea Res.*, **39**, 567–601.
- Opdyke, N.D., Kent, D.V. & Lowrie, W., 1973. Details of magnetic polarity transitions recorded in a high deposition rate deep-sea core, *Earth planet. Sci. Lett.*, **20**, 315–324.
- Perry, R.K., Flemming, H.S., Weber, J.R., Kristoffersen, Y., Hall, J.K., Grantz, A., Johnson, G.L., Cherkis, N.Z. & Larsen, B., 1986. Bathymetry of the Arctic Ocean, Naval Research Laboratory, Acoustic Division, printed by the Geological Society of America.
- Prévot, M., Mankinen, E.A., Coe, R.S. & Grommé, C.S., 1985. The Steens Mountain (Oregon) geomagnetic polarity transition 2. Field intensity variations and discussion of reversal models, *J. geophys. Res.*, **90B**, 10,417–10,448.
- Roperch, P., Bonhommet, N. & Levi, S., 1988. Paleointensity of the earth's magnetic field during the Laschamp excursion and its geomagnetic implications, *Earth planet. Sci. Lett.*, **88**, 209–219.
- Ryan, W.B.F., 1972. Stratigraphy of late Quaternary sediments in the Eastern Mediterranean, in *The Mediterranean Sea: A Natural Sedimentation Laboratory*, pp. 149–169, ed. Stanley, D.J., Dowden, Hutchinson & Ross, Stroudsburg, Pennsylvania.
- Sasajima, S., Nishimura, S. & Hirooka, K., 1984. The Blake geomagnetic event as inferred from Late Brunhes ignimbrites in Southwest Japan and West Indonesia, *J. geomagn. Geoelect.*, **36**, 203–214.
- Sejrup, H.P., Miller, G.H., Brigham-Grette, J., Løvlie, R. & Hopkins, D., 1984. Amino acid epimerization implies rapid sedimentation rates in Arctic Ocean cores, *Nature*, **310**, 772–775.
- Shibuya, H., Cassidy, J., Smith, I.E.M. & Itaya, T., 1992. A geomagnetic excursion in the Brunhes epoch recorded in New Zealand basalts, *Earth planet. Sci. Lett.*, **111**, 41–48.
- Smith, J.D. & Foster, J.H., 1969. Geomagnetic reversal in Brunhes normal polarity Epoch, *Science*, **163**, 565–567.
- Spielhagen, R., Pfirman, S. & Thiede, J., 1988. Geowissenschaftlicher Bericht über die ARK IV/3 Expedition des PFVS Polarstern im Sommer 1987 in das zentrale östliche Arktische Becken, Ber. Geol.-Paläont. Institut, Universität Kiel, **24**.
- Steuerwald, B.A., Clark, D.L. & Andrew, J.A., 1968. Magnetic stratigraphy and faunal pattern in Arctic Ocean sediments, *Earth planet. Sci. Lett.*, **5**, 79–85.
- Thiede, J. & ARK IV/3 Scientific Party, 1988. Scientific Cruise Report: ARK IV/3 expedition with the RV Polarstern, *Rep. Polar Res.*, **43**.
- Thompson, R. & Oldfield, F., 1986. *Environmental Magnetism*, Allen and Unwin, London.
- Thouveny, N., 1988. High-resolution palaeomagnetic study of Late Pleistocene sediments from Baffin Bay: first results, *Can. J. Earth Sci.*, **25**, 833–843.
- Thouveny, N., Creer, K.M. & Blunk, I., 1990. Extension of the Lac du Bouchet palaeomagnetic record over the last 120,000 years, *Earth planet. Sci. Lett.*, **97**, 140–161.
- Tric, E., Laj, C., Jéhanno, C., Valet, J.P., Kissel, C., Mazaud, A., Iaccarino, S., 1991a. High-resolution record of the upper Olduvai transition from Po Valley (Italy) sediments: support for dipolar transition geometry?, *Phys. Earth planet. Inter.*, **65**, 319–336.
- Tric, E., Laj, C., Valet, J.P., Tucholka, P., Paterne, M. & Guichard, F., 1991b. The Blake geomagnetic event: transition geometry, dynamical characteristics and geomagnetic significance, *Earth planet. Sci. Lett.*, **102**, 1–13.
- Tucholka, P., Fontugne, M., Guichard, F. & Paterne, M., 1987. The Blake magnetic polarity episode in cores from the Mediterranean Sea, *Earth planet. Sci. Lett.*, **86**, 320–326.
- Valet, J.-P., Tucholka, P., Courtillot, V. & Meynadier, L., 1992. Paleomagnetic constraints on the geometry of the geomagnetic field during reversals, *Nature*, **356**, 400–407.
- Verosub, K.L. & Banerjee, S.K., 1977. Geomagnetic excursions and their paleomagnetic record, *Rev. Geophys. Space Phys.*, **15**, 145–155.
- Westgate, J., 1988. Isothermal plateau fission-track age of the late

- Pleistocene Old Crow tephra, Alaska, *Geophys. Res. Lett.*, **15**, 376–379.
- Westgate, J., Walter, R.C., Pearce, G.W. & Gorton, M.P., 1985. Distribution, stratigraphy, petrochemistry, and palaeomagnetism of the late Pleistocene Old Crow tephra in Alaska and the Yukon, *Can. J. Earth Sci.*, **22**, 893–906.
- Whitney, J., Johnson, H.P., Levi, S. & Evans, B.W., 1971. Investigations of some magnetic and mineralogic properties of the Laschamp and Olby flows, France, *Quat. Res.*, **1**, 511–521.
- Wilson, D.S. & Hey, R.N., 1981. The Galapagos axial magnetic anomaly: Evidence for the Emperor event within the Brunhes and for a two-layer magnetic source, *Geophys. Res. Lett.*, **8**, 1051–1054.
- Witte, W.K. & Kent, D.V., 1988. Revised magnetostratigraphes confirm low sedimentation rates in Arctic Ocean cores, *Quat. Res.*, **29**, 43–53.
- Wollin, G., Ericson, D.B., Ryan, W.B.F. & Foster, J.H., 1971. Magnetism of the earth and climatic changes, *Earth planet. Sci. Lett.*, **12**, 175–183.
- Worsley, T.R. & Herman, Y., 1980. Episodic ice-free Arctic Ocean in Pliocene and Pleistocene time: calcareous nannofossil evidence, *Science*, **210**, 323–326.
- Yaskawa, K., Nakajima, T., Kawai, N., Torii, M., Natsuhara, N. & Horie, S., 1973. Paleomagnetism of a core from Lake Biwa (I), *J. geomagn. Geoelect.*, **25**, 447–474.
- Zahn, R., Markussen, B. & Thiede, J., 1985. Stable isotope data and depositional environments in the late Quaternary Arctic Ocean, *Nature*, **314**, 433–435.